MRES RESEARCH PROJECT:

Utilisation Of Fly Ash In The Manufacture Of Useful Materials

R Sommerville

[redacted]

Supervisor: - Dr N. Rowson

Abstract

Fly ash, if not utilised, is considered a waste product. Zeolitisation of coal fly ash offers the opportunity to create an added value product from a waste stream. Optimisation of the two-step zeolitisation process is necessary in order to render the process profitable. The Objective of this thesis is to analyse the optimisation of Si extraction from fly ash and the conditions of crystallisation. The type of synthetic zeolites produced were found to be highly dependent on the conditions of the crystallisation process, which has produced zeolite Na-P1, sodalite, zeolite Na-A, zeolite K-A and other species.

Crystallisation parameters explored by this thesis include pH, sodium aluminate addition, time at which ash and leachate are separated, length of crystallisation period, temperature, and control experiments on Si leaching from glassware. Further experimentation analysed the effects of a closed loop system on yield, variations in ash used in the leaching process, generation of floating zeolite via precipitation on cenospheres, highly caustic ash leaching, and Ga and Ge content analysis of ash leachate.

Eight sets of cation exchange capacity tests were carried out. Zeolite Na-P1, zeolite Na-A, sodalite, two samples of zeolitised ash, and three samples of unzeolitised ash were mixed with synthetic Acid Mine Drainage (AMD) at high and low solid loadings. Results were found to be heavily influenced by loading. AMD samples mixed with 2g/l zeolite Na-P1 were found to have complete Fe removal, 36% Zn removal, and 48% Mn removal after 160 minutes. 2g/l of zeolitised ash produced removals of 99%, 13% and 16% of Fe, Zn and Mn respectively, with 0.2g/l reducing content 15% and 4% for Zn and Mn respectively after 160 minutes. 0.2g/l of zolite Na-A reduced Fe, Zn and Mn by 14%, 10% and 20% respectively. It is noted that absorption is rapid, and results taken at 2.5 minutes are often similar to those taken at 160 minutes.

Acknowledgements

The author thanks the Engineering and Physical Sciences Research Council of the United Kingdom, RockTron Research Ltd, Dr N Rowson, R Blissett and S Savva.

Contents

List of Figures

List of Tables

Chapter 1

Introduction

1.1 Objectives

The overall objective of this thesis is to work towards the utilisation of improved fly ash residue in the production of synthetic zeolite. This is achieved by Precipitating synthetic zeolite from a solution of Si and Al. Therefore the first objective of this thesis is to optimise the extraction of Si into solution. After sufficient Si is in solution, the next objective is to optimise the crystallisation conditions to produce a good yield of the desired zeolite. The third objective of this thesis is to test the performance of the synthetic zeolite produced.

1.2 About Fly Ash

Fly ash (FA) is defined by European standard EN450 as a "fine-grained powder, which is mainly composed of spherical glassy particles, produced

during the combustion of pulverised coal" (1). The combustion of pulverised coal produces two main solid byproducts: bottom ash, and fly ash. Bottom ash remains at the bottom of the furnace, and is not the subject of this thesis. Fly ash, which forms between 60 and 88 wt% (2) of the solid residue is considered a pollutant if unused, and requires disposal (3; 4; 5).

1.3 Production

The main source of fly ash is from coal burning thermoelectric power plants. It is estimated that around 750 million tonnes (3) of fly ash are produced globally per year. In order to reduce harm to the environment and meet emissions standards, fly ash is removed from the flue gas, either by filtration using bag filters, cyclones or scrubbing with electrostatic precipitators (3; 4; 6).

1.4 Uses

Current uses for untreated fly ash include multiple applications as an aggregate and structural fill, such as landfill, land reclamation, minefill, embankments and road beds and pavement runways (1; 4). Other applications may involve some treatment of the fly ash but include brick manufacture, bitumin filler, ceramics, catalysts and catalyst supports, adsorbent for organic compounds and gas streams, a feedstock for acid leaching of metals, soil pH and clay amendment, chemical fertiliser and as a settling aid and chemical oxygen demand reducer (1; 4; 6; 7; 8; 9). One of the most common applica-

tions for coal fly ash is as a replacement for pozzolanic material in ordinary portland cement (OPC), due to the fine particle size and good binding properties. Various standards set limits on the amount of ash which can be used to replace OPC: EN197-1 (35%), ASTM C 595 (40%), ASTM C 1157 (unlimited), and ASTM C 618 (requirements to be established by testing) are four such standards. High Volume Fly Ash (HVFA) concrete contains over 50% fly ash and has many benefits, as listed by Blissett (2012) (3), including improved workability and early strength at 7 days, and improving strength between 28 and 90 days (3; 4). Coal fly ash can also be used as a feedstock for the manufacture of zeolites and mesoporous materials, which will be the focus of this thesis (1; 3; 10; 11).

Chapter 2

Material Overview

Coal fly ash is a grey, abrasive refacory powder with a predominantly fine particle size, but a wide particle size distribution. It is polycomponent, heterogeneous, and predominantly amorphous, but this varies greatly depending on coal type and combustion conditions. Fly ash is predominantly inorganic, with a variable carbon content (also dependent on combustion conditions) which when increased produces a darker coloured ash (2; 4). Particle size distributions are shown in figure 2.1.

2.1 Composition

Raw (untreated) fly ash consists of predominantly silica (SiO_2), alumina (Al_2O_3) and iron oxides (Fe_2O_3). The most common elements (>1%) are oxygen, silicon, aluminium, iron, calcium, magnesium, sodium, potassium, sulphur and carbon. The components of fly ash can be divided into three categories: material which is unaffected by the combusion process (primary),

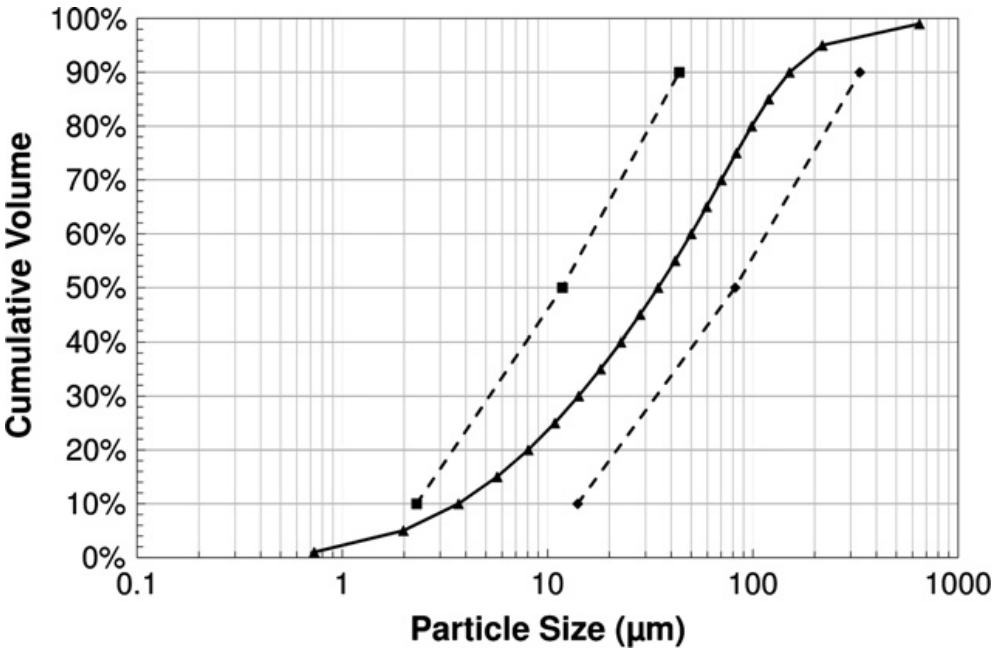

Figure 2.1: Particle size distributions of an UK CFA (▲) in comparison to upper (♦) and lower (■) ranges from 23 European CFAs (3)

material which is formed by the combustion process (secondary) and material which is formed by the storage and transportation process (tertiary) (2; 4; 6; 12). It is noted that the larger size fractions (above 43μm) are enriched in carbon, and that finer size fractions are enriched in trace elements, such as rare earth elements (13; 14). An elemental analysis of four ashes utilised and produced by RockTron is shown in table 2.1.

2.2 Separable Components of Fly Ash

2.2.1 Cenospheres

Cenospheres are small, hollow ceramic spheres, formed during the combusion process, thus they are secondary components of fly ash (see section 2.1), and

Table 2.1: Elemental Content of 4 ash samples, measured by Inductively Coupled Plasma - Optical Emission Spectroscopy. Results in wt % (14)

Oxide	Alpha	Delta	FB7	Lagoon
Al_2O_3	23.60 %	23.34 %	23.23 %	19.46 %
BaO	0.09 %	0.08 %	0.08 %	0.09 %
CaO	2.68 %	2.61 %	2.99 %	2.06 %
Cr_2O_3	0.02 %	0.01 %	0.02 %	0.01 %
CuO	0.02 %	0.01 %	0.01 %	0.01 %
Fe_2O_3	5.07 %	5.09 %	6.04 %	7.36 %
K_2O	3.94 %	3.04 %	2.90 %	2.68 %
MgO	1.35 %	1.37 %	1.72 %	1.26 %
MnO	0.05 %	0.07 %	0.11 %	0.06 %
Na_2O	2.44 %	2.03 %	2.29 %	2.06 %
P_2O_5	0.32 %	0.17 %	0.36 %	0.23 %
SO_2	0.10 %	0.04 %	0.08 %	0.05 %
SiO_2	41.60 %	43.68 %	38.97 %	44.03 %
SrO	0.05 %	0.03 %	0.06 %	0.04 %
TiO_2	0.38 %	0.31 %	0.36 %	0.30 %
V_2O_5	0.02 %	0.01 %	0.02 %	0.02 %
ZnO	0.20 %	0.13 %	0.23 %	0.22 %

their form and quantity will vary depending on coal type and combustion process. Due to the air trapped within the spheres, they have a low density. Literature defines cenospheres in different ways, but many opt for a measurement of density such as <2.2g cm^{-3} or <1g cm^{-3}. Cenospheres tend to be concentrated in the larger size fractions of the ash, with the smallest cenospheres noted to be around 4μm (1; 3; 12; 15; 16). Cenospheres are one of the most important components of fly ash due to their many high value applications which rely on their low density, including low density concrete, floating catalysts and lightweight composite materials (3).

2.2.2 Unburnt Carbon

Carbon forms up to 25% by mass of the ash, depending on coal and combustion conditions. Due to the "Clean Air Act" (1990) in the US, NO_x emissions are limited. In order to inhibit NO_x formation, cooler burning temperatures are used in the boilers. Cooler burning temperatures results in incomplete combustion of the coal, and lower efficiencies, raising the carbon content of the fly ash. The unburnt coal contains (as well as carbon) oxygen, nitrogen, sulphur and hydrogen. Carbon Concentrates (CC) separated from the fly ash has a calorific value of 5000-6000 kcal kg^{-1}, a specific surface area of 10-134 m^2g^{-1}, and a density of 0.26-0.28 g cm^{-3}. Particle Size Distribution (PSD) tests show that larger fractions contain the majority of the carbon (3; 4; 7; 14; 17). Unburnt carbon has a variety of uses. It can be re-used as a fuel in the combustion process, selling for a value comparable to that of coal, it can be used as a feedstock for the production of activated carbon for a variety of applications or graphite for Li-ion batteries (3).

2.2.3 Magnetics

The magnetic content of fly ash is another component which will vary depending on coal and combustion conditions, and can vary between 0.5% and 18%. A magnetic concentrate can be recovered which is primarily spherical iron enriched aluminosilicate with an iron content of 20-61% by weight, and low LOI (1.8%, compared to 4.9% for untreated FB7 fly ash), indicating good separation between carbon and magnetic concentrates (3; 2; 14; 17). The magnetic concentrate has a variety of uses, including as dense medium

separation in coal cleaning circuits, fillers for polymers and composite materials, recording medium, and have various specialist applications due to their high density and electromagnetic properties (3).

2.2.4 Strategic Metals

Gallium and Germanium have been identified as critical strategic metals by an EU comission, which notes that the EU is heavily dependent on external sources for these metals (3). It is noted that concentrations of such metals can be raised in coal ashes. Germanium extraction yields of over 90% and gallium extraction yields of 60-86% can be achieved (18; 19; 20).

2.3 RockTron Process

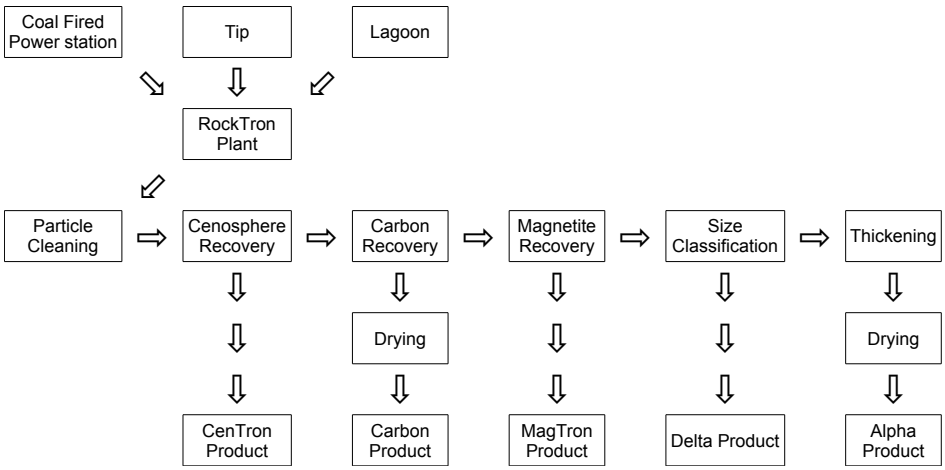

Figure 2.2: A Summary of The RockTron^{TM}Process (14; 21)

Figure 2.2 shows a summary of the RockTron process. The ash is received either directly from the plant, or from storage. The cenosphere recovery step

is a simple sink/float separation, which assumed that all cenospheres have a density of <1g cm^{-3}. Carbon is recovered through froth flotation, which exploits the hydrophobic nature of the carbon to float it to the top. Repeated froth flotation steps are utilised to increase the concentration of both carbon concentrate, and reduce the amount of carbon left in the ash. Magnetite is recovered using wet magnetic separation to produce the magnetic concentrate. The remaining ash, which has had cenospheres removed, and carbon and magnetic components reduced, then undergoes a size classification to separate coarse material (delta) from fine material (alpha) which is then thickened to remove water, and finally dried.

2.3.1 Alpha Product

The alpha product, made by RockTron, is one of the main feedstocks used for experiments in this thesis. It consists of predominantly silica and alumina, with a carbon content of below 5%, and a reduced iron content. The small particle size (below 43 μm) combined with the reduction of carbon and iron content increases the reactivity of the ash, making it an acceptable partial or possibly even complete substitute for OPC.

2.3.2 Delta Product

The delta product, made by RockTron has been through the same cenosphere removal, carbon reduction and magnetite removal processes as the alpha product, and thus has a very similar content, albeit at a larger size fraction. Main applications for the delta product are as an aggregate or a filler. Due

to the large particle size, delta is not considered reactive enough to be used as a replacement for OPC.

Chapter 3

Zeolitisation

3.1 Zeolite Description

A zeolite is defined in *Introduction to Zeolite Science and Practice* as "A crystalline aluminosilicate with a three-dimensional framework structure that forms uniformly sized pores of molecular dimensions" (22). The framework consists of tetrahedra of $[SiO_4]^{4-}$ and $[AlO_4]^{5-}$ linked at each point by the oxygens they share. The structure includes group I or II element counter-ions, which can be swapped out to allow for cation exchange. The substitution of Si^{4+} for Al^{3+} results in a net negative charge, as shown in figure 3.1 which shows the zeolite structure (1; 6; 22; 23).

3.2 Motivation for Zeolitisation

Zeolitisation of fly ash provides an opportunity to produce an added value product from a waste stream. Due to the three-dimensional framework, and

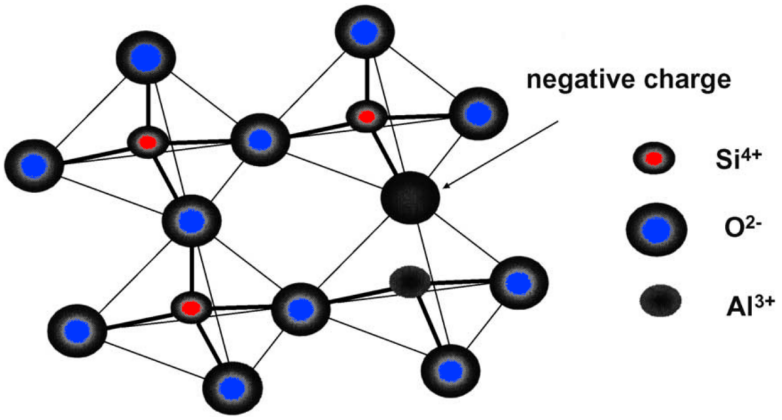

Figure 3.1: Theoretical zeolite structure, showing tetrahedral units and negative charged induced by Silicon/ Aluminium substitution (1)

the voids in it which allow easy access to molecules, zeolites have high cation exchange capacities of up to 5meq g^{-1} (1; 23). This high cation exchange capacity can lend zeolites to a variety of uses, including but not limited to detergents, gas absorption (such as carbon capture), water purification, soil improvement, and utilisation of zeolites as molecular sieves to remove metals in the remediation of acid mine drainage. Although zeolites do occur naturally and are mined for use, it has been found that the sorption capacity of synthetic zeolite "NaP1" is 10 times greater than natural zeolite, thus the synthetic zeolite has clear advantages over natural alternatives (1; 3; 10; 24; 25; 26; 27; 28; 29).

3.3 Zeolitisation

In order to synthesise zeolites, a source of silica and alumina is needed to form the material itself. Coal fly ash, being made up of mostly silica and alumina is ideal for this. There are various methods available to rearrange

the silica and alumina into zeolites, as shown in figure 3.2. The Hydrothermal method, which involves synthesis in an alkaline environment at an elevated temperature has shown to have been successful in the past. The time taken for the hydrothermal zeolitisation step to complete is highly variable, taking anything from hours to months (1; 6; 22; 24; 26; 30; 31).

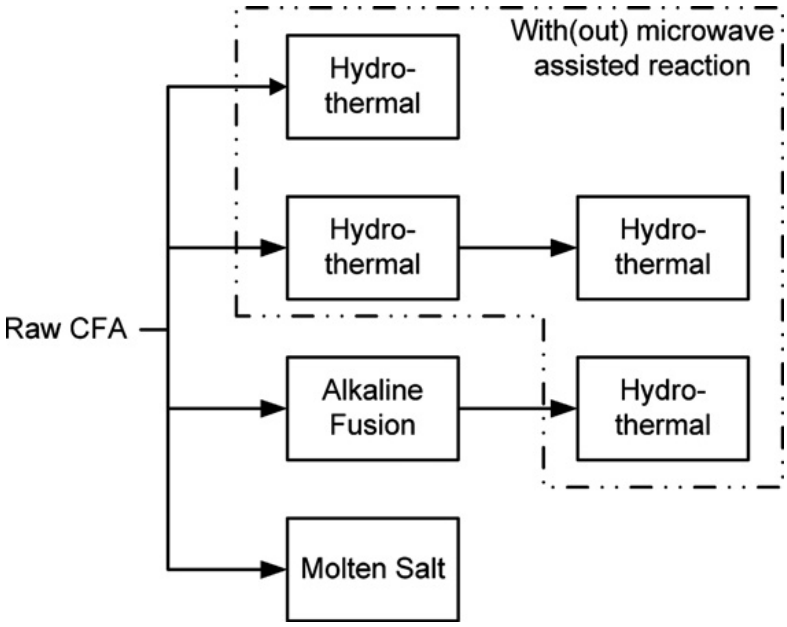

Figure 3.2: Various experimental approaches to the manufacture of zeolites from coal fly ash (3)

3.3.1 One Step Zeolitisation

The one step zeolitisation process involves the aforementioned mixing of fly ash with hot NaOH in order to extract the Si and Al into solution, and then adding a source of aluminium (such as sodium aluminate from Al etching plants) (3) in order to get the correct Si/Al ratio for the precipitation of various zeolites. This solution is then incubated at a high temperature which

causes zeolite to crystallise out of solution and form on the surface of the ash. The result is ash coated in zeolite. In previous studies when this product was added to syntheic acid mine drainage it was shown to reduce the Fe, Zn and Mn content (14).

3.3.2 Two Step Zeolitisation

The two step zeolitisation process of Hollman et al (32) uses a process similar to the one step zeolitisation process, except the fly ash is filtered out of the solution. This leaves a solution rich in Si, to which the Al can be added in order to precipitate a high purity zeolite. An advantage of this two step process is that it removes the possibility of hazardous leachable elements such as Mo, As, Cr and V leaching into solution from the fly ash still present in the product, as may be the case with the one-step zeolitisation method (1).

Chapter 4

Experimental Work

4.1 Equipment

Figure 4.1 shows the equipment used for the zeolitisation and crystallisation experiments. The apparatus consisted of a round-bottomed 1l pyrex leaching vessel, with a 100mm bore flat flange for connection to a flat flanged Pyrex lid with 5 socket joints (3 shown in diagram). The leaching vessel was heated by an electric heating mantle, and the contents of the vessel were mixed using a PTFE coated stirrer and a Heidolph mixer at 325 rpm. The temperature of the vessel's contents were measured using a mercury thermometer with a range of 0-110°C.

4.2 Process

Figure 4.2 shows the process flow diagram for the two step zeolitisation process. Variables for optimisation are shown in grey. For the leaching step,

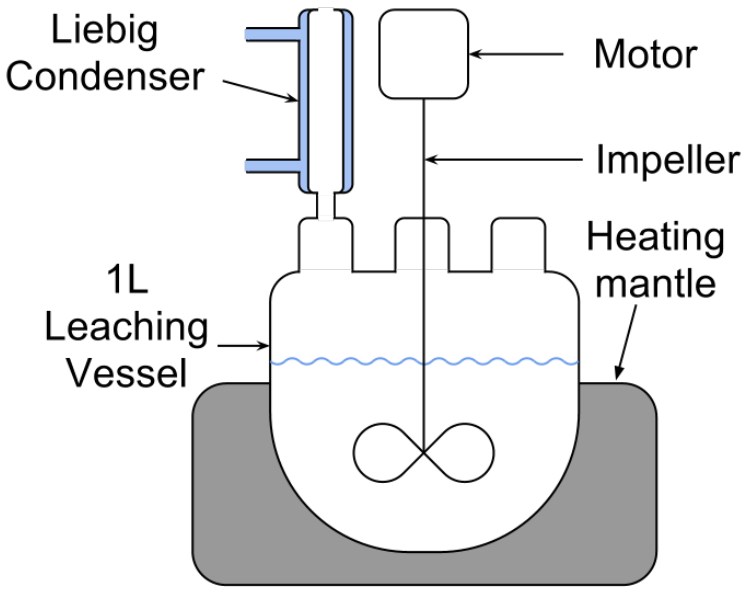

Figure 4.1: Diagram of equipment used in leaching and crystallisation processes

variables were:

- Quantity of ash used
- Type of ash used
- Concentration of NaOH solution
- Amount of heat applied to system
- Length of experiment

Constants were:

- Volume of solution used (1l)
- Impellor mixing speed (˜325rpm)

The ash was then separated from the first leachate (Leachate 1 or L1) using a sintered glass Büchner funnel. For the leaching process, the variables were:

- Concentration of L1 used (dilution with distilled water)

- Amount of sodium aluminate added (dissolved in distilled water)
- Amount of heat applied to system
- Length of experiment

Total volume and impellor mixing speed were again kept constant. As with the leaching step, at the end of the experiment, any precpitate can be filtered out using a Büchner funnel to separate the syntheic zeolite from Leachate 2 (L2).

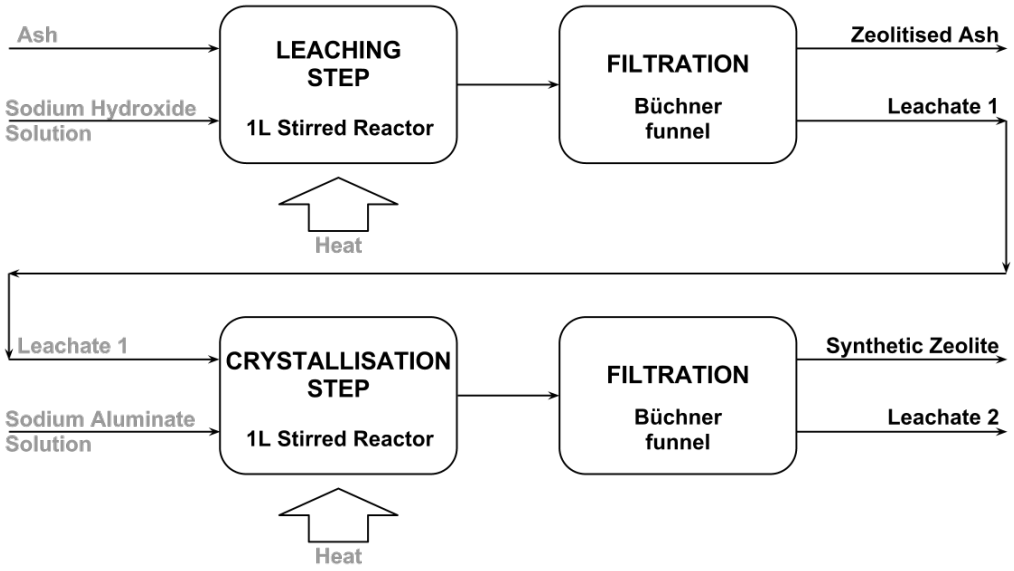

Figure 4.2: Process flow diagram of the two step zeolitisation process, with variables for optimisation shown in grey

4.3 Scoping Experiments

The conditions for the scoping experiments continued with the solids loading and NaOH concentrations used in previous experiments (14), as shown in table 4.1.

Table 4.1: Scoping experiment conditions

Ref	Solids (g/l)	Temp (°C)	NaOH (M)	Time (h)
SE1	225	95	2	6
SE2	225	95	2	6
SE3	225	95	2	12
SE4	225	95	2	6

4 Scoping experiments (SC1-4) were carried out. Crystallisation experiments were carried out using the entirety of L1, with no added aluminium or distilled water the day after the leaching experiment (with the exception of SE1, which was carried out a few days after the leaching step), at 95 °C for 6 hours. In the scoping experiments and first leaching experiments a water bath, rather than heating mantle, was used. The experiments were identical, except for the delay for SE1, and the length of SE3.

4.4 Leaching Experiments

Optimisation experiments were carried out on the leaching step to ascertain the optimum conditions for solids loading, temperature, and sodium hydroxide concentration. Using principles from the design of experiment module, the three conditions were varied between a high and a low point, with a midpoint of all taken, and repeated. Thus, the solids loading of alpha ash was varied between 100g/l and 400g/l, NaOH was varied between 0.5M and 4M, and temperature was varied between ambient and reflux conditions, as shown in table 4.2.

Table 4.2: Leaching optimisation experiments

Ref	Solids (g/l)	Temp (°C)	NaOH (M)
000	100	20	0.5
001	100	20	4
010	100	100	0.5
011	100	100	4
100	400	20	0.5
101	400	20	4
110	400	100	0.5
111	400	100	4
LH1	250	60	2.25
LH2	250	60	2.25

These experiments were conducted twice, once in the autumn term, using a water bath, for 12 hours, and again in the spring term, using a heating mantle, for 4 hours.

For each experiment, the NaOH solution was heated (if necessary) until no further temperature change was noted. At this point, the ash was added to the leaching vessel using a funnel and the timer started. At regular intervals, 25ml samples of ash suspension were taken using a syringe and plastic tubing, from the same depth within the vessel at each extraction. The sample was deposited into a 25ml plastic sample pot and allowed to settle for approximately 20 minutes. The fluid from the top of the settled sample was taken up into the syringe and then forced through a syringe filter into another sample pot for later analysis. At the end of the experiment, the heat source was turned off, the Büchner funnel assembled, and the contents of the leaching vessel filtered to separate the zeolitised ash from the primary leachate (L1). A sample of L1 was then set aside for later analysis, and distilled water used to wash through the zeolitised ash.

4.5 Crystallisation Experiments

Details of the conditions for crystallisation exeperiments are shown in table 4.3 on page 29. The table shows the main variable being analysed by each experiment, the reference number of the experiment, the concentration of NaOH in the leaching step (M), the amount of sodium aluminate (SA) added to the crystallisation step (g) and the concentration of L1 in L2 (i.e: a 50% concentration contains 500ml of L1 and 500ml of distilled water to make L2), the temperature at which the crystallisation step took place, and the length of time it was carried out for. All experiments were conducted using the equipment shown in figure 4.1, using a heating a mantle. All leaching experiments used the conditions from experiments "011" from the leaching tests, i.e: 100g/l of ash, reflux conditions, and 4M NaOH, with the exception of SC2, SC9, SC26 and SC27, which used 8M NaOH. The leaching process was the same as for the leaching optimisation experiments, except no samples were taken during the leaching process, L1 was retained, the majority of the zeolitised ash discarded.

4.5.1 Leaching Si from Glassware

Experiment SC0 was conducted to ascertain how much Si was leached from the pyrex by the hot NaOH during leaching and crystallisation. This experiment was conducted without the addition of any ash to the leaching step, but otherwise the crystallisation step was the same as for the other experiments.

4.5.2 Effects of Dilution of L1

The first two crystallisation experiments (SC1 and SC2) were conducted using all of L1 from the leaching step, with no added distilled water (except for 50ml of distilled water used to dissolve SA). All other experiments henceforth (with the exception of the 8M NaOH leaching experiments) were conducted using 500ml of L1 and 500ml of L2. The leaching experiments which used 8M NaOH (SC2, SC9, SC26 and SC27) used 250ml of L1, and 750ml of distilled water.

4.5.3 Sodium Aluminate Addition

In order to assess the impact of the quantity of SA added, experiments SC3, SC4, SC6 and SC7 were conducted. In each of these, an increasing concentration of SA solution was added to the crystallisation step. SA added was 1.6g, 4g, 8g and 16g for experiments SC3, SC4, SC6 and SC7 respecitvely.

4.5.4 Time of Filtration

Due to fears that temperature of filtration may influence Si content of L1 and L2, for experiments SC10-SC30, unless otherwise stated, experiment procedure was updated to the following proceedure. At the start of the leaching process, 160g of NaOH was added to 800ml of distilled water in the leaching vessel, and mixed. Upon complete dissolution of the NaOH pellets, the heating mantle was turned on, and the contents of the leaching vessel allowed to reach just in excess of 100 °C. At this point, the ash was added, and 200ml of distilled water used to wash any remaining ash into the vessel. At

the end of the experiment, the heat source was turned off, and the experiment left mixing for 5 minutes. After 5 minutes the mixer was turned off and the leaching vessel was removed from the heat source, and left, unmixed for a further 15 minutes. 20 minutes after the end of the experiment, the contents of the leaching vessel were poured into the running Büchner funnel. This filtration process applied for both leaching and zeolitisation steps. For the crystallisation process, 500ml of L1 and 300ml of distilled water were added to the leaching vessel and heated to over 100 °C with the mixer running. In the case of the 8M leach experiments (SC2, SC9, SC26, SC27), 250ml of L1, and 550ml of distilled water were added to the leaching vessel. Once the leaching vessel contents had reached over 100 °C, 200ml of SA solution were poured into the vessel, and the timer started.

4.5.5 Length of Crystallisation

Experiments SC10-SC14 investigated the effect of time, following statements by Jha et al (23) that reaction time positively affects zeolitisation. Experiments were carried out at 3, 6, 24 and 48 hours. These results were compared to SC6, which is considered a benchmark, at 12 hours. The 48 hour crystallisation step is repeated twice (SC12, SC14), as SC12-L2 was accidentally discarded before a sample could be saved, thus was not available for AAS analysis.

4.5.6 Temperature

Three Experiments (SC15, SC17 & SC19) were conducted in order to analyse the impact of temperature on the crystallisation step. These were conducted at ambient temperature (˜25°C), 50°C, and 75°C, then compared to SC6, which was conducted under reflux.

4.5.7 Closed Loop System

In order to minimise costs, it may be more efficient to use L2 as a feedstock for the leaching step. Thus, the secondary leachate (L2) from experiments SC16, SC18 and SC20 was recycled and used as feed for the leaching process for experiments SC18, SC20 and SC22. Due to the dilution between leaching and crystallisation, it was necessary to measure the pH (via titration with phenolphthalein) and add more NaOH. For the sake of simplicity, it is assumed that the colour change occurs at pH 7, and that the reaction of HCl with NaOH is equimolar. After the 25ml sample for analysis has been taken, and the volume of L2 made up to 1l with distlled water, a 1ml sample of this now slightly diluted L2 in 50ml of distilled water was titrated with 0.5ml of phenolphthalein and 0.1M HCl. The amount of NaOH present in the slightly diluted L2 solution was compared to a fresh leaching solution with 160g of NaOH dissolved in 1l of distilled water. The molarity of NaOH in the slightly diluted L2 was then adjusted to be equal to the molarity of NaOH in the fresh sample.

4.5.8 Floating Zeolites

In experiments SC21, SC23, SC24 and SC28, an attempt was made to create floating zeoltie. 12.5g, 25g, 50g and 100g of cenospheres were added to the mixture of L1 along with the distilled water, and heated to over 100 °C, after which the crystallisation step carried on as per normal. As it was suspected that a greater yield of Si in L1 may be produced were L1 to be separated from the zeolitised ash whilst still hot, an adjustment was made to the experimental method in these experiments. For experiments SC21, SC23, SC24 and SC28, the filtration step was completed within five minutes of the end of the experiment (referred to as hot filtering). It was expected that any change in Si content which may influence yield would be evident in the AAS analysis of L1.

4.5.9 Source Ash

Experiments SC8 and SC25 used raw fly ash (FB7) and delta ash respecitively as the feedstock ash, rather than alpha ash.

4.5.10 Highly caustic leaching

Experiments SC2, SC9, SC26 and SC27 were conducted to assess the influence of 8M NaOH rather than 4M NaOH, following statements by Jha et al (23) that increased alkali concentrateion increases dissolution of Si and Al, and also hastens zeolite formation. In SC2, L1 was not diluted before crystallisation. Experiments SC9 and SC27 are essentially the same, except for the time of filtration. SC9 was not controlled, and SC27 was controlled,

filtering being completed within five minutes of the end of the experiment. For the crystallisation step, SC9 had 8g of SA added, whereas SC27 had 4g added. SC26 used the same conditions and filtering time as SC27, except the feed ash was delta, rather than alpha.

4.5.11 Other Experiments

In an attempt to address the apparent instant crystallisation observed when SA solution is added to crystallisation solution, it was decided to add the SA solution in repeated, small aliquots in experiment SC29. 20g of SA was dissovled in 50ml of distlled water, and 12.5ml (5g) aliquots were added every 3 hours.

In order to address the wastage of some of L1 between the leaching and crystallisation steps for a closed loop system, concentrated H_2SO_4 was added in order to neutralise some of the NaOH. 30ml of concentrated sulphuric acid were added dropwise to ambient temperature L1 and distilled water in a water bath before being heated up for the crystallisation step.

4.5.12 Particle Size Analysis

In order to ascertain the particle size distribution of the products of crystallisation, each solid sample was measured for its particle size distribution using a Mastersizer 2000, with distilled water as the dilution medium.

4.6 Cation Exchange Capacity

In order to analyse the cation exchance capacity (CEC) of the products of these experiments, they were mixed with synthetic acid mine drainage containing Fe, Zn and Mn. This method is similar to one utilised in previous work (14), albeit using sythetic, rather than authentic acid mine drainage. 1000ppm solutions of Fe(III), Zn(II) and Mn (II) were created, and their pH measured. A solution containing 25ml of Fe solution, 30ml of Zn solution and 5ml of Mn solution was made up to 1l with distilled water, and adjusted to have a similar pH (˜2) to the most acidic solution of the three 1000ppm starting solutions, using concentrated sulphuric acid.

8 materials were selected for analysis. These materials were:

- Zeolite P
- Zeolite A
- Sodalite
- Zeolitised Ash from 8M NaOH leaching conditions
- Zeolitised Ash from 4M NaOH leaching conditions
- Alpha Ash
- Untreated FB7 Ash
- Delta Ash

The absorbency of each material was tested at two solids loadings: 2g/l and 0.2g/l. Every 1l batch of syntheic acid mine drainage (AMD) created was divided into two 500ml aliquots. Each material was tested using at high and low solids loading using two 500ml aliqutos from the same batch. Before solids were added, a 25ml sample was taken from the high solids loading

sample for reference as an untreated sample. The synthetic AMD and solids were put into 1l Pyrex Duran bottles, and mixed on a tumbling mill. As absorption was expected to be pseudo-first order (26), the measurements were taken with focus on the start of the experiment, at 2.5, 5, 10, 20, 40, 80 and 160 minutes from the start of the experiment. The experimental method was as follows:

- Remove bottle from tumbling mill
- Use a disposable 50ml pipette to take 25ml sample from Duran bottle and deposit into a 100ml glass beaker.
- Dry pH and temperature probes and put into the glass beaker, note time, and put Duran bottle back on tumbling mill.
- Note pH 15 seconds after probes are inserted into glass beaker
- Remove pH and temperature probes, and take sample into 25ml syringe
- Force contents of syringe through syringe filter into sample pot
- Rinse pH meter into glass beaker with distilled water
- Rinse glass beaker with distilled water
- Dry glass beaker ready for next sample

In order to account for the effects of the solid samples raising the pH of the synthetic AMD and metals precipitating out of solution as mentioned by Querol et al (1) and Moreno et al (30), a set of neutralisation experiments were conducted. As a scoping run, a beaker with 100ml of synthetic AMD was placed on a magnetic stirrer, with pH and temperature probes inside. A solution of 0.01M NaOH was added from a 50ml pipette, with approximate pH and volume of NaOH added thus far noted at regular pH intervals of

0.3. The experiment was then repeated. This time, a fresh 100ml aliquot of synthetic AMD was placed in the measuring beaker each time, the majority of the NaOH required to reach the desired pH was quickly added in order to save time, then the final ˜5ml of NaOH were added dropwise to slowly approach the desired pH. Samples were taken in increments of 0.3 between pH 2 and pH 5, and saved for later AAS analysis.

Table 4.3: Crystallisation optimisation experiments

Variable	Ref	NaOH (M)	SA (g)	L2 Conc. (%)	Temp °C	Time (h)	Detail
Blank	SC0	4	8	50	100	12	No ash added
Undiluted L2	SC1	4	20	100	100	12	No dilution
Undiluted L2, 8M	SC2	8	1.65	100	100	12	No dilution, 8M leach
Sodium Aluminate	SC3	4	1.6	50	100	12	
Sodium Aluminate	SC4	4	4	50	100	12	
AAS of L1	SC5	4					
Sodium Aluminate	SC6	4	8	50	100	12	STANDARD
Sodium Aluminate	SC7	4	16	50	100	12	
Ash	SC8	4	8	50	100	12	FB7 as source ash
8M	SC9	8	8	25	100	12	
Time	SC10	4	8	50	100	3	
Time	SC11	4	8	50	100	6	
Time	SC12	4	8	50	100	48	
Time	SC13	4	8	50	100	24	
Time	SC14	4	8	50	100	48	
Temp	SC15	4	8	50	25	12	
Recycle	SC16	4	8	50	100	12	
Temp	SC17	4	8	50	50	12	
Recycle	SC18	4	8	50	100	12	
Temp	SC19	4	8	50	75	12	
Recycle	SC20	4	8	50	100	12	
Seeds	SC21	4	8	50	100	12	12.5g Cenospheres
Recycle	SC22	4	8	50	100	12	
Seeds	SC23	4	8	50	100	12	25g Cenospheres
Seeds	SC24	4	8	50	100	12	50g Cenospheres
Ash	SC25	4	8	50	100	12	Delta as source ash
8M, Ash	SC26	8	4	25	100	12	Delta as source, 8M
8M	SC27	8	4	25	100	12	Alpha as source, 8M
Seeds	SC28	4	8	50	100	12	100g Cenospheres
Incremental Al	SC29	4	20	50	100	12	Al added incrementally
Undiluted L2, Acid	SC30	4	8	50	100	12	Conc. H_2SO_4 added

Chapter 5

Analysis Techniques

5.1 Colourimetry

Colourimetry exploits the absorption of light by elements in a solution to analyse the content of a particular fluid for a given element. In the case where the element itself does not absorb light, or does not absorb enough light to be easily measured, the element can be complexed with others which do absorb light. The amount of light absorbed at a given wavelength will be directly proportional to the concentration of the element present, and can thus be measured against a set of standards of known concentration and a blank (33).

5.2 X-Ray Fluorescence

X-Ray Fluorsecence is a method used to analyse the elemental composition of a sample. This is achieved by exciting electrons in the sample and mea-

suring the characteristic frequency of the x-rays which are released. X-rays are commonly generated from an x-ray tube, but radioisotopes, synchrotrons and scanning electron microscopes can also be used (34; 35; 36; 37). Figure 5.1 shows how the x-ray beam excites one, or multple electrons, temporarily raising them to higher shells, before the electrons fall back to lower shells, each releasing an x-ray (known as fluorescence) of a frequency which is indicative of the energy difference of the shells between which the electron fell (35; 37; 38; 39). Figure 5.2 shows an example of an XRF analysis device. The

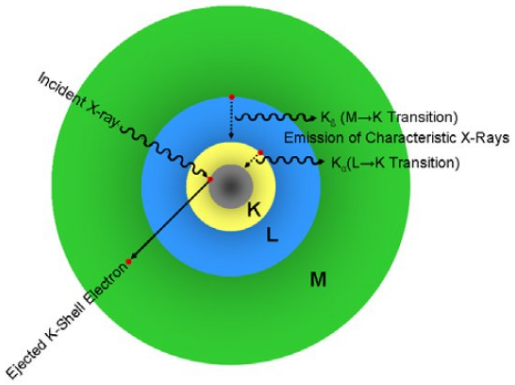

Figure 5.1: X-ray fluorescence principle (35)

x-ray source in this case is an x-ray tube. Generated x-rays are directed at the sample, which fluoresces, the x-rays from which pass through the collimator, are diffracted by the analyser crystal, and are then measured by the gas proportional counter and scintillation counter (35; 37; 38; 40). The intensity and frequencies of the x-rays measured are shown on a spectra, such as figure 5.3. This figure shows how elements such as iron have multiple peaks. At a frequency of around 6.4 KeV there is a peak marked "Fe KA1". KA, or Kα electrons have fallen from the L-shell into the K-shell. At around 7.1 KeV there is another peak labelled "Fe KB1". KB, or Kβ electrons have fallen

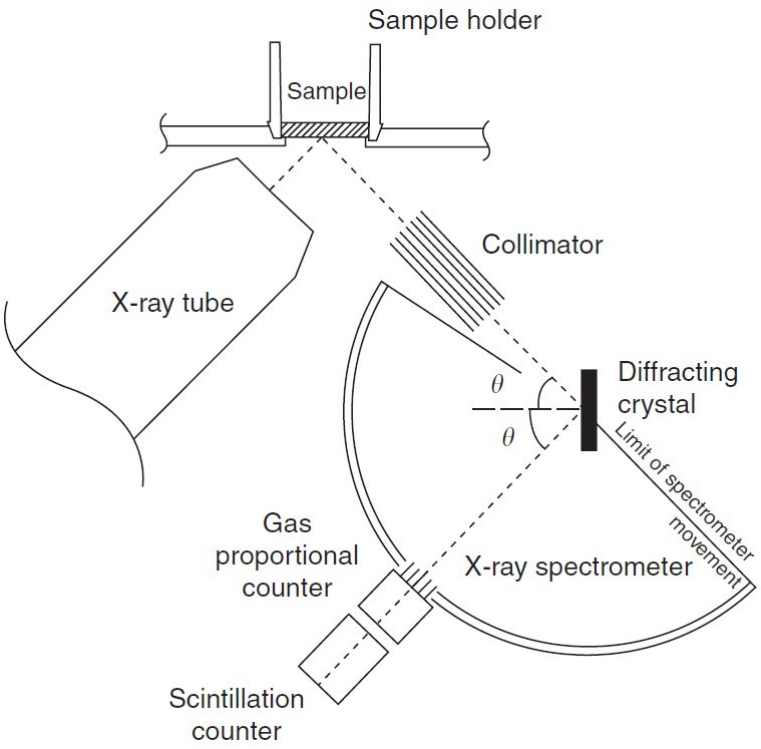

Figure 5.2: X-ray fluorescence equipment setup (40)

from the M-shell into the K-shell, as shown in figure 5.1. At a frequency of 0.7 KeV there are two Fe peaks overlapping each other, marked "Fe LA1" and "Fe LB1". These indicate electrons which have fallen from the M shell to the L shell and the N shell to the L shell respectively. The letter indicates the shell to which the electron has fallen, and the Greek letter the number of shells by which it has fallen. The greater the intensity of the measurement of an x-ray at a given frequency, the higher the concentration of the element in the sample being analysed. Thus, XRF gives not only qualitative (position of peaks) but quantitative (height of peaks) analysis of the sample. The height of one peak relative to another does not indicate a higher concentration of one element than another. Some frequencies will naturally produce stronger

signals than others, thus frequency is taken into account when calculating elemental content.

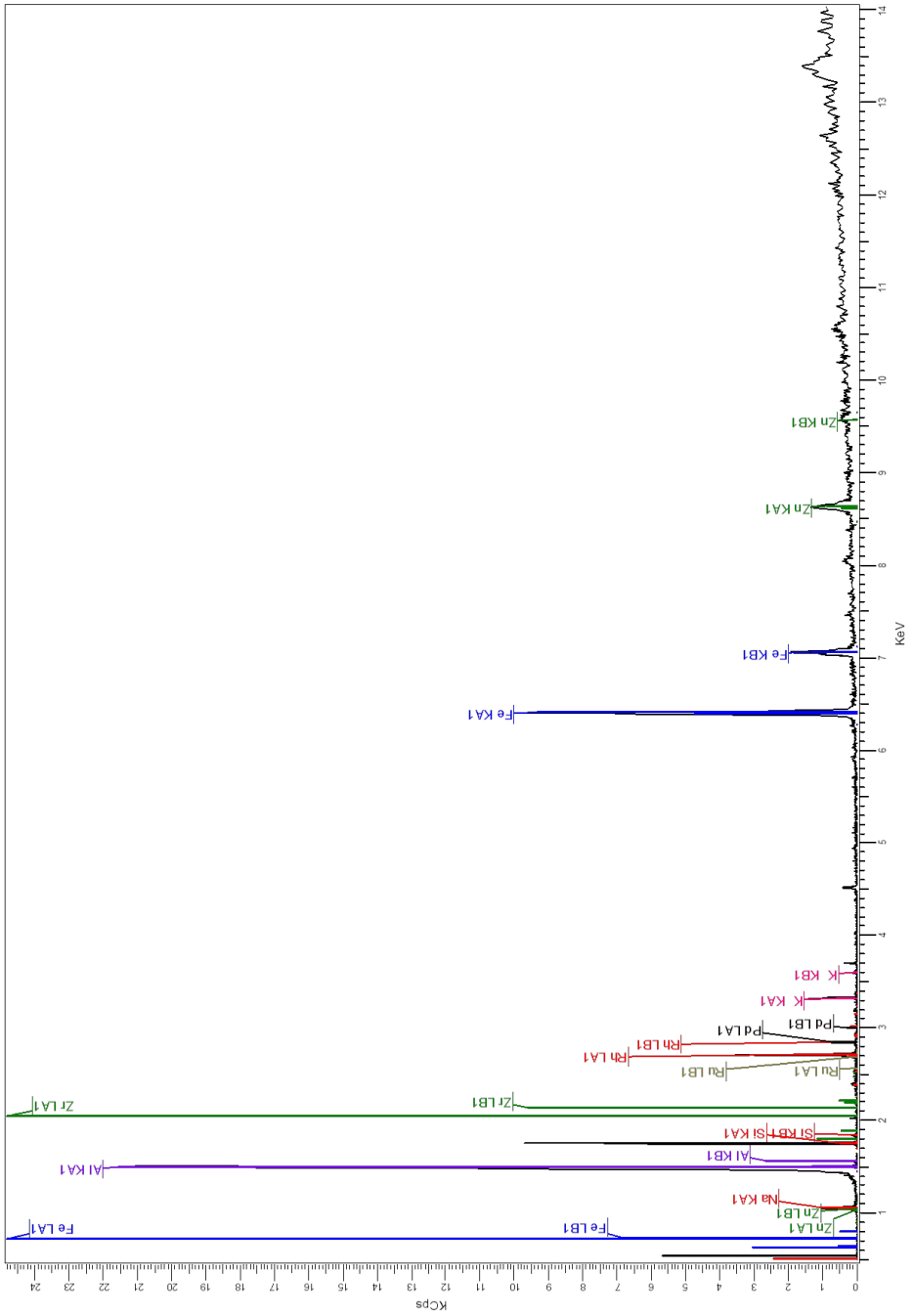

Figure 5.3: X-ray fluorescence on synthetic zeolite sample SE2-Z

5.2.1 Advantages & Disadvantages

XRF analysis is limited to heavier elements. Lighter elements are harder to analyse accurately, due to the weak intensity of x-rays evolved. In order to increase detection, a helium atmosphere (helium will diffract x-rays less than air) or vacuum can be used to increase sensitivity. The lightest elements cannot be analysed with XRF at all (34). The best results are attained from flat, polished surfaces, thus sample preparation can be fastidious. In terms of zeolite samples, the best results would be attained by melting the zeolite with flux to form a glass which is allowed to cool. This sample would then be known as a fused bead, however making fused beads is costly and slow. Results of an accuracy sufficient for this thesis can be achieved by mixing the zeolite powder with wax to make a pressed pellet (assuming sufficient sample volume), which is compressed at around five tonnes. This produces a smooth, flat surface which provides reasonable XRF analysis. XRF analysis of both fused beads and pressed pellets of fly ash have been conducted, and whilst fused beads are more accurate, costly and time consuming, for the sake of brevity, the comparison of their accuracies has been omitted.

5.3 X-Ray Diffraction

X-ray diffraction provides a method of analysing the lattice structure of a sample by measuring the distances between atomic nuclei, thus offering an insight into the crystalline structure of the sample (41). As with XRF, X-rays are generated by a source, are aimed at the sample, hit the sample and are scattered back. Some of these x-rays which are scattered back will hit the

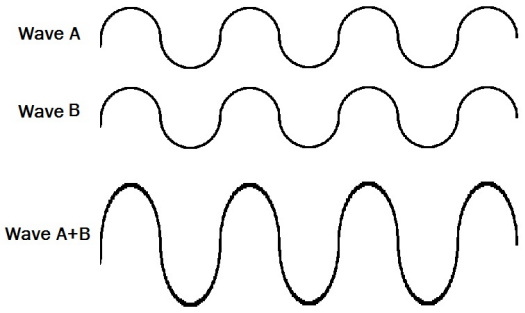

(a) Constructive Interference

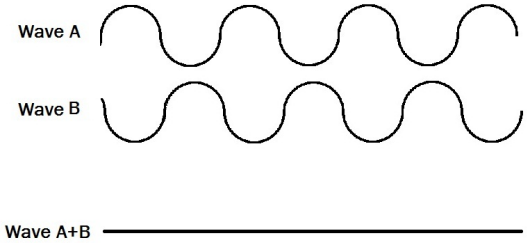

(b) Destructive Interference

Figure 5.4: Constructive and destructive wave interference

detector. When the x-rays hit the sample, depending on the spacings of the atoms in the lattice, their orientation to the incident beam and the frequency of the x-rays, x-rays may undergo constructive interference, (see figure 5.4) and the amplitude of the x-rays hitting the detector increases. The intensity of an x-ray measured by the detector is proportional to the square of the amplitude of the wave, thus areas which produce constructive interference produce a sudden "spike" in the x-ray signal, compared to the "background" the rest of the time.

Figure 5.5 shows how the x-rays may interact with the sample being analysed. The figure shows three layers of atoms, $d\mathring{A}$ apart. The incident x-ray from the top left, strikes two atoms, and x-rays are reflected toward the top

right. Both of the x-rays are at an angle θ relative to the sample. XRD relies on Bragg's law to find d, knowing θ and λ, which is the wavelength of the x-ray. Bragg's law states: $\lambda = 2d \sin\theta$, thus the angles (θ) at which high intensity readings of x-rays are found for constant λ, d can be derived (38; 41; 42; 43).

As various crystal forms will have different values for d, they will pro-

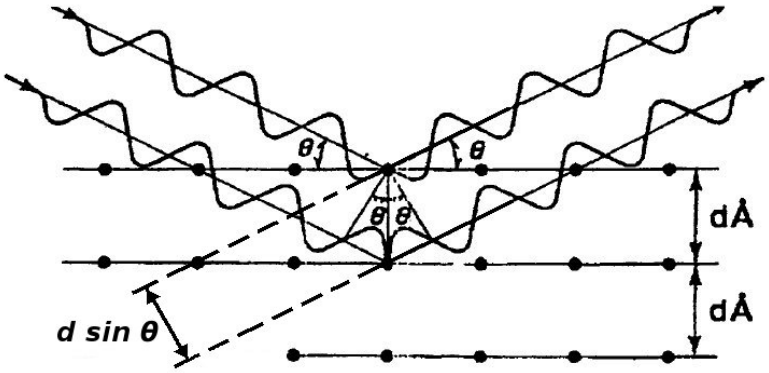

Figure 5.5: X-ray diffraction principle, lattices and interference (42)

duce high intensity peaks at different values for θ. The θ values at which the high intensity measurements were found can be compared with around 75000 known samples in a database compiled and maintained by the JCPDS (Joint Committee on Powder Diffraction standards) (38; 41; 43).

5.4 Atomic Absorption Spectrophotometry

Atomic Absorption Spectrophotometry (AAS) is a method used to analyse the elemental content of a liquid sample. Figure 5.6 shows the setup for an atomic absorption spectrophotometer. An aliquot of sample is taken up in

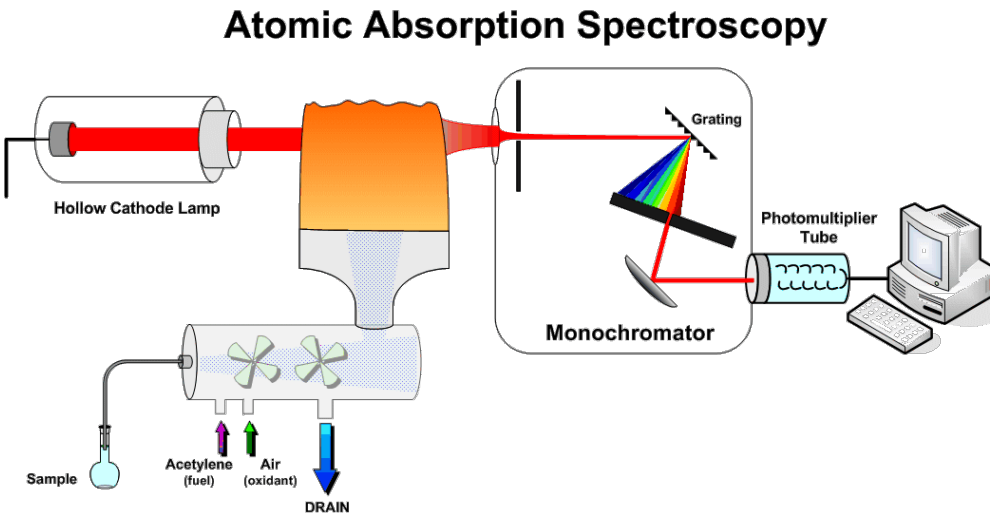

Figure 5.6: Atomic Absorption Spectrophotometer Diagram (44)

to the nebuliser. In the nebuliser, the sample is mixed with the fuel and oxidant. The specific fuel and oxidant used will depend on the equipment being used, and the sample being analysed. Certain elements (such as Si) will require a higher flame temperature for reliable analysis. Acetylene is a commonly used fuel. In cases where a higher flame temperature is required NO_2 can be used in lieu of air as the oxidant in order to attain a higher flame temperature. The sample is aspirated into the flame where the sample is atomised. A hollow cathode lamp contains a cathode of the element to be analysed. The cathode is bombarded by energetic Ne^+ or Ar^+ ions to excite the electrons of the atoms in the cathode. The electrons then return to their ground state, and in doing so emit light of a wavelength which is specific to the cathode's element. The light emitted from the cathode is directed through the flame containing the atomised sample. The atomised sample will absorb some of the light from the cathode, and the rest of the light will pass through the flame. After passing through the flame, the light

passes through a monochromator. The monochromator serves to filter out all light which is not of a specific wavelength. The monochromator will be set to filter out all light which is not of the wavelength specific to the element being analysed, thus should only allow through light of the same wavelength as that which is emitted by the hollow cathode lamp at the far left of figure 5.6. The output of the monochromator may then be passed through a photomultiplier in order to increase the intensity of a given reading for better accuracy. The intensity of the light exiting the photomultiplier is proportional to the light transmitted through the flame. Transmittence of light through the flame will be inversely proportional to absorbence of light by the atoms in the flame, which will be proportional to the concentration of atoms in the flame. The Beer-Lambert law states that transmittence can be related ot the concentration of the sample through the molar absorption coefficient: $T = \frac{I}{I_0} = e^{-\alpha' l} = e^{-\sigma l C}$, where:

- T = Transmission
- I = Intensity of incident light
- I_0 = Intensity of transmitted light
- α' = Absorption coefficient
- l = Distance travelled through flame
- σ = Absorption cross section
- C = Concentration of absorbing particles

Thus, knowing the length of the flame, and cross sectional area of the beam of light, the concentration of sample in the flame can be derived, which can then be related to the concentration of that element in the original sample (33; 44).

Chapter 6

Results & Discussion

6.1 Introduction

In this chapter the restults of the aforementioned experiments are discussed. The four scoping experiments are discussed first, followed by the Si extraction experiments on page 41. A control experiment analysing Si extraction from glassware is on page 43, followed by analysis of the effects of dilution, sodium aluminate addition, time of filtration, length of crystallisation, temperature, using a closed loop system, floating zeolites, changing the source ash, highly caustic leaching and other experiments on pages 44 to 70. This is followed by the analysis of the zeolites which were produced on page 75, and their performance in cation exchange capacity tests on page 78.

6.2 Scoping Experiments

Of the four scoping experiments, two produced a precipitate: SE2 (0.317g) and SE4 (0.389g). The precipitates formed were white powders. XRD analysis of these precipitates indicated that they were both zeolite Na-P1. With the exception of the delay between leaching and crystallisation for SE1, experiments SE1, SE2 and SE4 all had the same method. The leaching step for experiment SE3 was 12h long, rather than 6h long for the other three experiments. It is theorised that any zeolite which could have been precipitated out during the crystallisation step was precipitated out onto the surface of the ash during the leaching step, leaving insufficient materials in solution for crystallisation after filtering. AAS analysis of later leachate samples shows that the Al content of Leachate 1 is generally quite low in comparison to the Si content. It is possible that the Al crashed out of solution during SE1's interim period, thus resulting in no yield following crystallisation. For SE3 it is possible that crystallisation of zeolite on the surface of ash particles consumed the little Al which was present, leaving the primary leachate with insufficient Al for the crystallisation step. Particle size analysis for the scoping experiments is shown in figure 6.1. The particle size analysis of the samples showed the D_{10}, D_{50} and D_{90} of the samples to be 5.751, 54.486, 555.895 μm for SE2 and 4.581, 39.004, 85.495 μm for SE4. This indicates a fine particle size for both experiments, but with a large tail for experiment SE2. This large tail on SE2 may be due to measurement error, through contamination with the previously measured sample (SC30) not being properly washed out of the mastersizer.

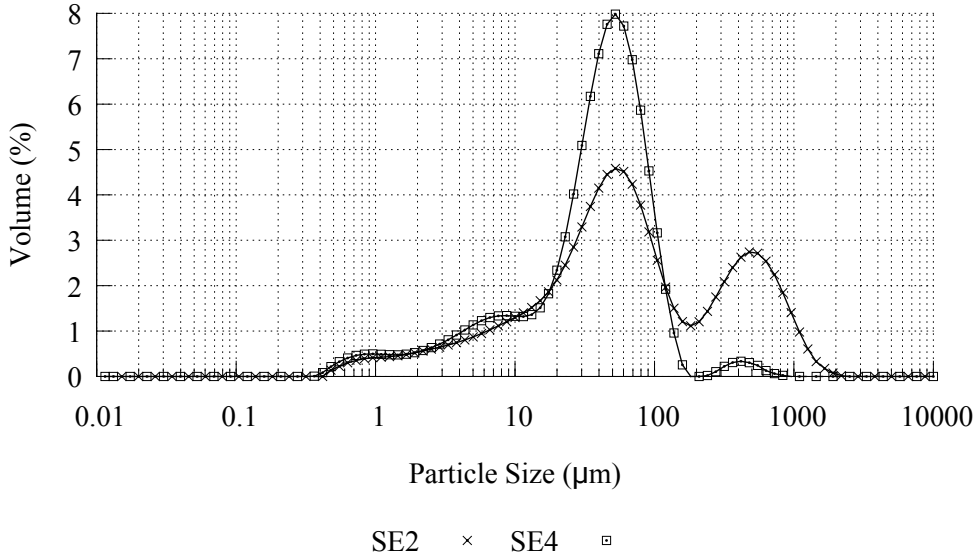

Figure 6.1: Particle size distribution: SE2 & SE4

6.3 Leaching Experiments

6.3.1 Colourimetry

The samples taken in the autumn term were measured using colourimetry, and analysed using a Jenway 6300 spectrophotometer. Figure 6.2 shows the results. Conditions for the experiments can be found in Table 4.2. The graph shows that some conditions (011, 111) produce notably higher Si levels than the rest. It was expected that the Si levels for each condition would stabilise within the 12 hours of the experiment, but this does not appear to be the case, as there are wide variations (clearest in the conditions with the highest Si levels: 011 and 111) in the Si levels. It should be noted that the final leachate is modelled as being a sample taken at 13h. Due to the results not stabilising it was postulated that the results may be unreliable, and repeated

analyses of two experiments were conducted.

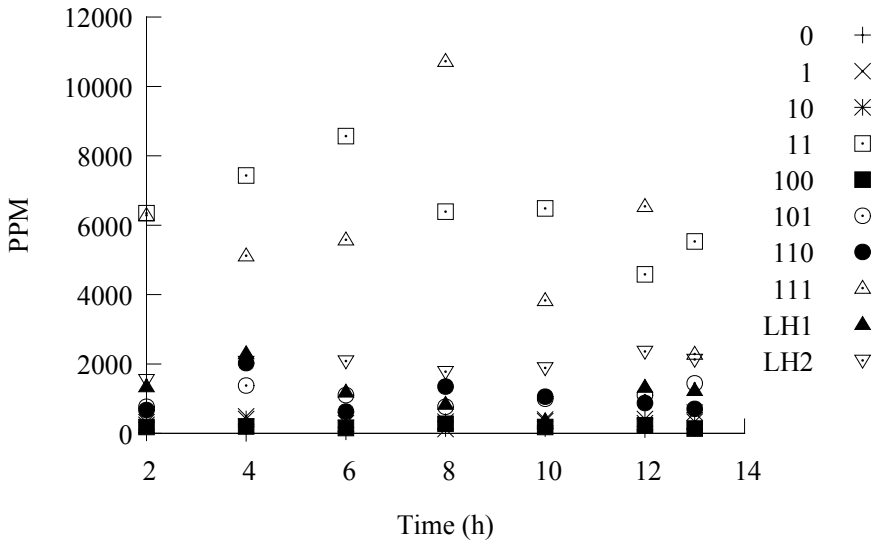

Figure 6.2: Autumn Si colourimetry analysis: all results

Figure 6.3 shows the repeatability of analysis for autumn experiments 011 and LH2. From these graphs it is clear that the repeatability was quite poor, and the experimental method and/or analysis technique should be improved.

The second set of leaching experiments were only conducted for 4h, rather than 12h. It was assumed that any stabilisation which may occur, would do so within the first 4 hours of the experiment. As with the Autumn results, the final leachate is also analysed, but modelled as being a sample taken at 4.5h. The Spring optimisation experiments were analysed using a silicomolybdate colourimetry method which involved less dilution of the original sample in order to bring them into the range which the photospectrometer could analyse them rather than the colourimetry method in the autumn experiments. The autumn results were used to calculate the order of magnitude by which the

samples should be diluted. The analysis method was also altered such that time was more vigorously controlled, and each sample was analysed as close to fifteen minutes after complexing as possible.

The results are shown in figure 6.4a. Results for conditions 000 and 110 are not shown, as these were all zero values. The results appear to have much less variation within each condition. Experiment 011 clearly produces the highest yield of Si, being double the next highest result. In most cases, there appears to be no obvious difference between the final measurement taken (4h) and the leachate (modelled as 4.5h). This indicates that the effect (if any) which Büchner filtration has on the final sample is comparable to the effects (if any) of syringe filtration. The repeatability of the results is also much improved, as shown in figure 6.4b. Standard deviations on the repeated analysis of the experiment with conditions 101 are between 40 and 90ppm, where the results are between 200 and 700ppm.

6.4 Crystallisation Experiments

6.4.1 Leaching Si from Glassware

AAS analysis of L1 (see figure 4.2) from experiment SC0 (see table 4.3) showed an Si content of 0.82 g/l, Al content of 0.05g/l and Na content of 102.37 g/l. When compared to other results where ash was used for leaching, the Si content of the leachate is quite low. Comparison of Si content in L1 in comparison to other experiments is shown in figure 6.12. The aluminium

content, although quite low, was higher than expected. Although this is the first crystallisation experiment discussed, it was conducted after experiments SC1-SC30, thus the aluminium content could be due to SA or zeolite which had crystallised on the inside of the vessel during previous experiments being re-dissolved. These values are expected to be higher than the actual values of Si or Al leached from the glassware during leaching or crystallisation experiments, due to the lack of ash present. After SA was added and the crystallisation step had run to completion, a 1.2g yield of Sodalite was produced. The particle size produced was found to be quite coarse compared to other precipitates, with the D_{50} at 116 μm. The PSD is shown in figure 6.5.

6.4.2 Effects of Dilution of L1

Experiments SC1 and SC2 used the entirety of L1, with no added distilled water. SC1 produced 31.68g of sodalite from the crystallisation step, where 20g of SA were added. The author theorised that the ratio of Al to Si was too high to precipitate zeolite Na-P1 (as was precipitated in scoping experiments SE2 and SE4). For this reason, in SC2, the ash was leached at 8M in order to rasie the Si content of L1, and then only 1.65g of SA were added. This produced a yield of 3.28g of Sodalite. Scoping experiments SE2 and SE4 used 2M NaOH in the leaching process, from which L1 was not diluted before crystallisation and zeolite P1 was produced. From this reference point, it was theorised that NaOH content of crystallisation solution influences which zeolite is precipitated. In order to recreate the results from the scoping

experiments, it was decided that future 4M leaching experiments would be diluted by 50%.

The partice size distribution graphs shown in figure 6.6 show a larger average particle size, with a narrower distribution for experiment SC2. It is also noted that for experiment SC1, the leachage instantly turned cloudy white upon the addition of the SA, indicating instant precipitation. The PSD indicates that instant precipitation and consumption of most of the Si and Al may well be the case due to the fine particle size. These results are in agreement with Jha et al (23), who stated that ash treated with 3.5 M NaOH produced sodalite, in comparison to ashes treated with 2M NaOH, which produce zeolite Na-P, and Querol et al (1) and Murayama et al (10), who produced zeolite P at NaOH concentrations of 0.5-3M, but hydroxysodalite at 3.0-5.0M NaOH and 4M NaOH respectively, with the highest intensity of zeolite P in crystallised products being produced from experiments with 2M NaOH (1; 10; 23).

6.4.3 Sodium Aluminate Addition

The dilution of L1 with distilled water did produce zeolite Na-P1, thus the scoping experiments were successfully recreated with an optimised leaching step and added aluminium. As the the amount of SA added increased, the yield increased, up to a maximum of 14.3g for 8g of SA added. Further addition of SA resulted in production of a mixture of zeolite Na-A and sodalite (or ZK-14; see section 6.5.2), with a yield of 13.9g. Production of zeolite P at higher Si/Al ratios and sodalite at decreased Si/Al ratios is confirmed by Jha et al (23).

Table 6.1: Effect of SA addition on yeild and zeolite produced

Experiment	SA (g)	Yeild (g)	Analysis
SC3	1.6	1.9	Na-P1 + Unknown
SC4	4	6	Na-P1 + K-A
SC6	8	14.3	Na-P1 + K-A
SC7	16	13.9	Na-A + ZK-14

Figure 6.7 shows the amount of Si and Al in the crystallisation step, before and after the 12h crystallisation experiment. The "start" values were calculated from AAS analysis of L1 samples. As only 500ml of L1 was used, and SA was added, these AAS values were adjusted to create these values shown, which are the estimated values for Si and Al in the crystallisation experiment. The "end" values were taken directly from the AAS analysis. AAS was not carried out on any experiments prior to SC4, thus no values are available for SC3.

It is noted that in every case the Si and Al content decreases during the crystallisation step. For SC4 and SC6, althought the Si content decreases, the Al content decreases to a much lower concentration, potentially slowing down or stopping crystallisation due to a lack of free Al in solution. In the case of SC7, both Si and Al appear to drop to a similar level.

Following addition of SA to the solution, there was no noticable immediate change in appearance. With the 8g dosage, the solution was clouded by the time the entirety of the SA was added to solution, and the same applies for the 16g dosage. This may indicate immediate crystallisation or precipi-

tation. Length of crystallisation experiment is discussed in section 6.4.5. It should be noted that despite similar leaching conditions, the Si content of SC4, SC6 and SC7 prior to crystallisation is not the same. This is discussed in the next section.

The PSD shown in figure 6.8 indicates that as SA addition increases, the particle size distribution broadens, and then average particle size decreases. This indicates a faster crystallisation, as would be expected, from a higher Al content as mentioned in section 6.4.2.

6.4.4 Time of Filtration

Variations were noted in the Si content of L1 in experiments SC4, SC5, SC6 and SC7, despite leaching conditions being the same. It was postulated that this could be due to the temperature at which L1 is filtered. Namely, that if L1 was left to cool before filtering, some of the Si would come out of solution resulting in a lower availability for the crystallisation step. The following experiments were filtered 20 minutes after the end of the experiment. Figure 6.9 shows the concentration of Si in L1 samples, as measured by AAS for 22 experiments. The first experiments, SC4, SC5, SC6 and SC7 do not have a controlled time of filtration and thus have a wide variation in Si contents. SC10-SC17, SC19, SC25 and SC29 all used the method explained in section 4.5.4. SC10-SC17 all have very similar concentrations of Si, around 6.2 g/l, indicating a much improved repeatability. SC10 was the first experiment us-

ing the new filtration method, and was filtered 10 minutes after the end of the experiment, rather than 20, as the rest, and thus has a slightly lower value than SC11-17. SC19 and SC25 have higher results than expected and SC29 has a lower result than expected. The variations in SC25 and SC29 may be put down to the use of Delta rather than Alpha as feed resulting in quicker draining through the Büchner funnel. The variation in SC19 is put down to inaccurate timekeeping resulting in early filtration. Experiments SC0, SC21, SC23, SC24 and SC28 were all filtered within five minutes of the end of the experiment. SC0 was the blank run, which contained no ash, and is included for reference. Time of filtration of SC9 was not controlled, but SC27 was. Both of these experiments were leached at 8M and are included for reference. Mean values for the different conditions and standard deviations therefrom are shown in table 6.2.

Table 6.2: Average and standard deviations of Si content in L1

Filtration	Experiments	Mean Si Conc. (g/l)	Standard Deviation (g/l)
Uncontrolled	SC4, SC5, SC6, SC7	10.12	2.24
20 Min filter (All)	SC10-SC17, SC19, SC25, SC29	6.58	1.56
20 Min (Excl. Anomalies)	SC10-SC17	6.26	0.09
5 Min (Excl SC0)	SC21, SC23, SC24, SC28	8.03	0.91

It is noted that the AAS values for L1 vary from the colourimetry values from the leaching optimisation experiments. As the time of filtration is clearly an influence on the Si content, and the leaching optimisation experiments did not have a controlled time of filtration, the colourimetry values may still be accurate. Irrespectively, the leaching optimistation experiment

results are taken as relativistic, rather than absolute.

6.4.5 Length of Crystallisation

The experiments analysing the length of the crystallisation step were SC10-SC14, with SC6 and/or SC16 as a benchmark. Table 6.3 shows how the length of the crystallisation step influences the type and yield of zeolite produced. Although experiments SC6 and SC16 are very similar, SC6 does not have a controlled time of filtration, whilst the others do, thus potentially explaining the variation in zeolite formed. It should be noted that the zeolite LTA and zeolite K-A are not high in concentration, and are only impurities, as shown in section 9.

Table 6.3: Influence of length of crystallisation step on yield and form of zeolite

Exp	Time (h)	Yeild (g)	Analysis
SC10	3	6.5	Na-P1 + LTA
SC11	6	13.6	Na-P1
SC6	12	14.3	Na-P1 + K-A
SC16	12	14.4	Na-P1
SC13	24	14.5	Na-P1 + K-A
SC12	48	14.2	Na-P1
SC14	48	15	Na-P1

The 12h benchmark is repeated twice, as SC6 was part of the SA dosage experiment run, and SC16 is part of the closed loop system experiments, both of which, for those experiments use the same conditions as as these time optimisation experiments. The 48 hour experiment was repeated twice,

as L2 was discarded in error for SC12. It shows that for the 3h crystallistaion step, the yeild is reduced from the standard of around 14.3g, but that the 6h experiment is already quite high, at 13.6g, whilst the longer experiments produce a slightly higher yield than the standard.

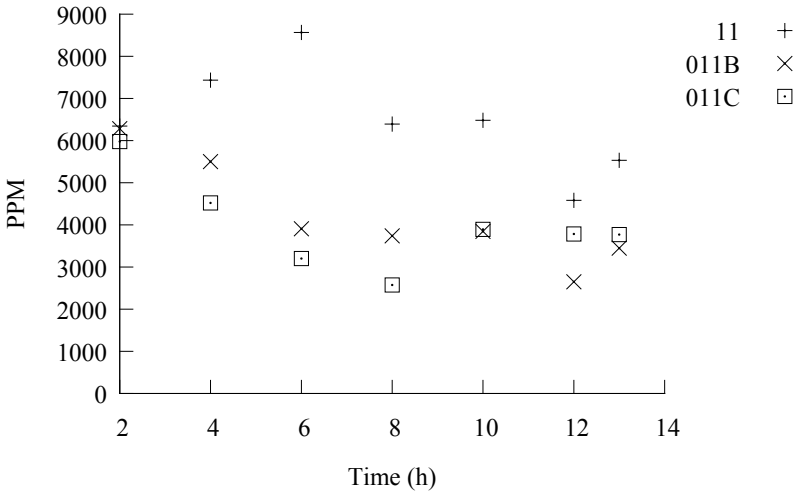

(a) Exeriment 011

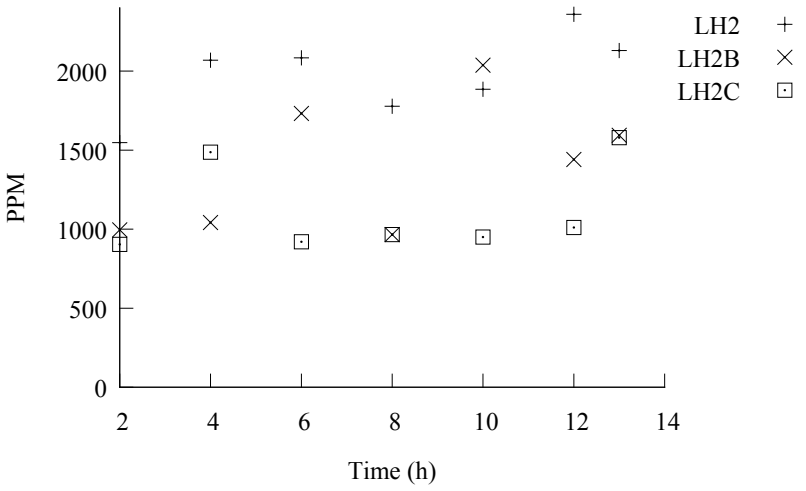

(b) Experiment LH2

Figure 6.3: Autumn Si colourimetry analysis: repetition

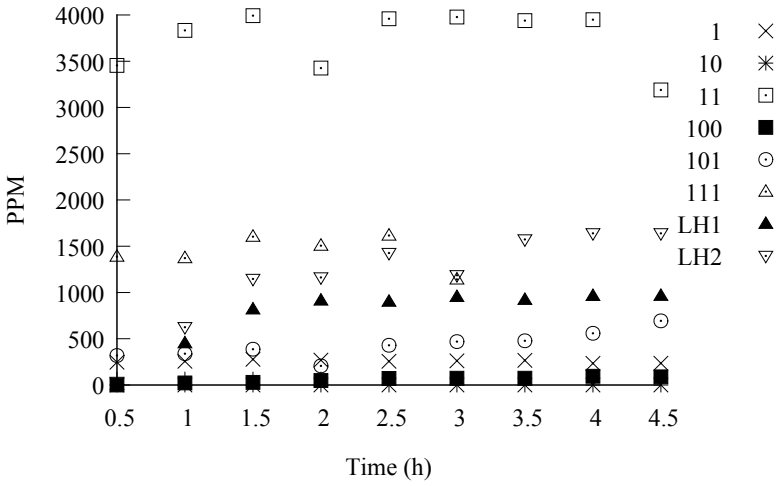

(a) All Results

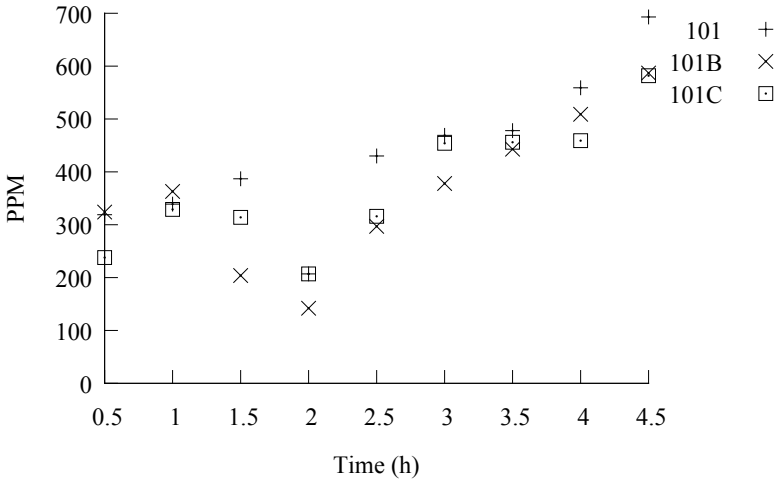

(b) Repeatability on Experiment 101

Figure 6.4: Spring Si colourimetry analysis

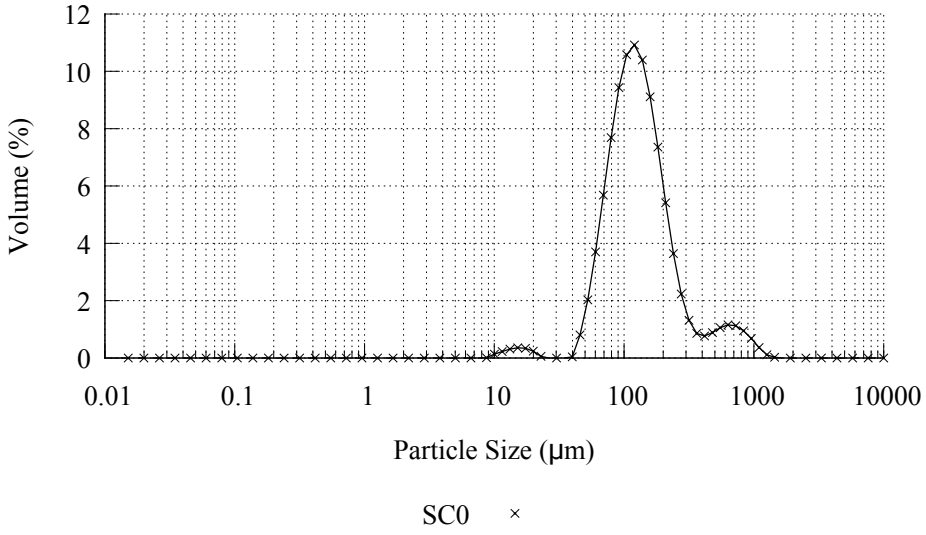

Figure 6.5: Particle size distribution: SC0

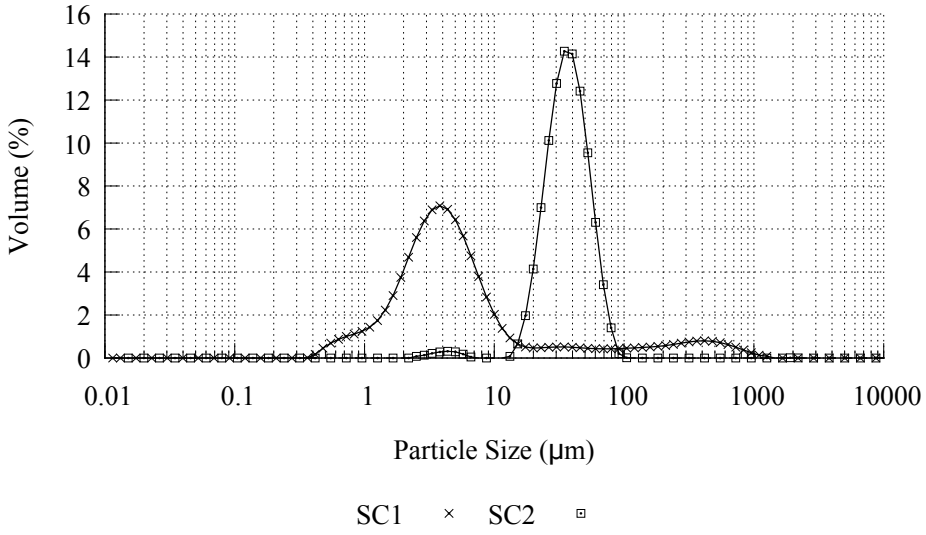

Figure 6.6: Particle size distribution: SC1 & SC2

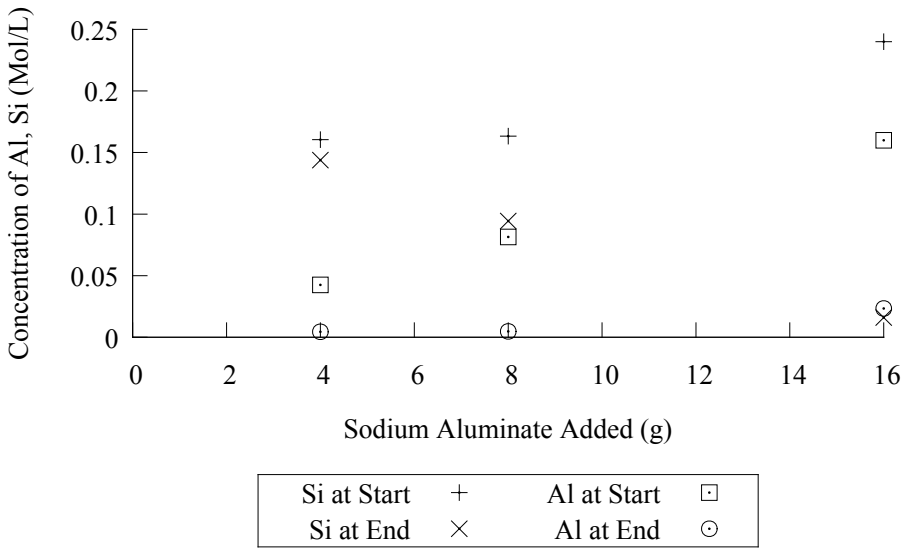

Figure 6.7: Si and Al content of L2 before and after crystallisation step: SA addition

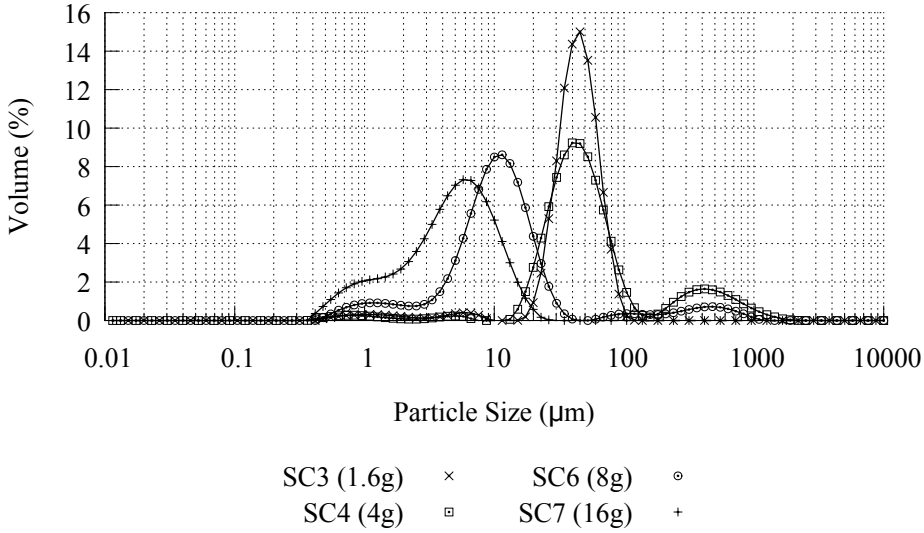

Figure 6.8: Particle size distribution: SC3, SC4, SC6 & SC7

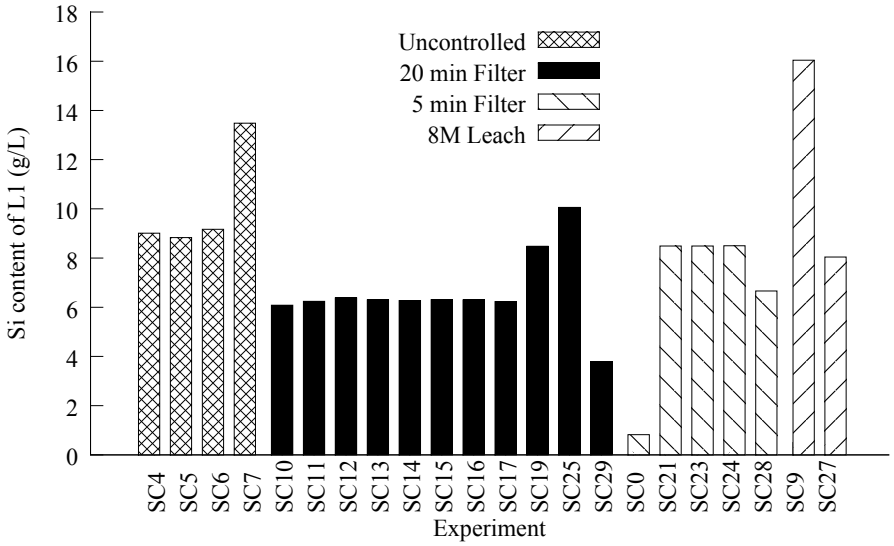

Figure 6.9: Effect of time of filtration

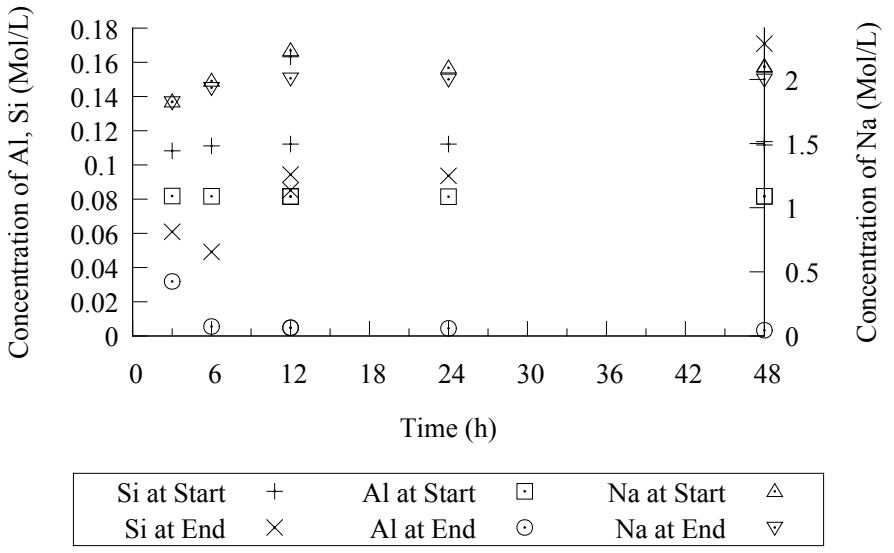

Figure 6.10: Effect of length of crystallisation step on Si, Al, and Na in solution

Figure 6.10 shows the effect that the length of the crystallisation step has on the Si, Al and Na in the crystallisation solution. The data shows the Si, Al and Na content in L2 at the start of the crystalisation step, calculated from AAS readings of L1, and the concentrations at the end, taken directly from AAS results. With the exception of a duplicate value at 12h (from SC6), the Si content at the start of each step is quite uniform, owing to the adjusted filtration timings. The Al content at the start of each experiment is also constant, with no obvious exceptions. By the end of the experiments, the Al concentrations in all samples has dropped. With the exception of the 3h experiment, all have dropped to a very low level. This indicates that the majority of the Al is consumed between 3 and 6 hours into the experiment. With the exception of the 48 hour experiment, the Si content has also dropped in all experiments. The drop is greatest in the 6h and then the 3h experiment. The large increase in Si content in the 48 hour experiment was not anticipated, but may be put down to leaching of Si from glassware over a long time period, or errors in the AAS analysis. The Na content of the 3h experiment drops insignificantly, whilst the other experiments do exhibit a decrease in Na content with time.

From the PSD graph shown in figure 6.11, the general trend shows that longer crystallisation periods tend to produce larger crystals in a smaller size range. The exception to this trend is SC6, where filtration time was not controlled, thus starting conditions are not necessarily the same for SC6 as for the other experiments in this run. It is also noted that SC6 produces a different result to SC16, which had similar conditions. There is little difference between the 24 and 48 hour experiments in terms of distribution of

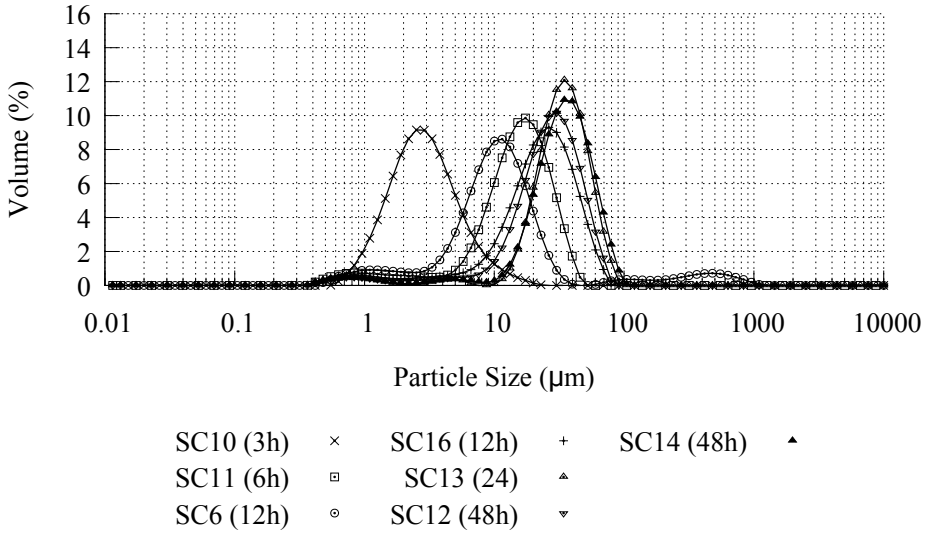

Figure 6.11: Influence of length of crystallisation step on Particle size distribution

particle size and average particle size. The widest particle size distribution, and the one with the smallest average size is SC10, which was 3h long. This is followed by SC6 (12h), and then SC11 (6h). Following these results, the 12h, 24h and 48 hour experiments are all grouped close together, with similar average sizes, and similar size distributions.

6.4.6 Temperature

The effects of the temperature of crystallisation on yield and form of zeolite are shown in table 6.4. This table shows that at lower temperatures, (25°C and 50°C), rather than forming crystalline zeolite, only amorphous material is formed. As temperature increases to 75 °C, crystalline material is formed, but as with the 25°C and 50°C experiments, the yield is lower than the benchmarks, under reflux (modelled as 100°C) which have the highest yields.

Table 6.4: Influence of temperature on yield and form of zeolite

Exp	Temp °C	Yield (g)	Analysis
SC15	25	8.4	Amorphous
SC17	50	9.1	Amorphous
SC19	75	8.2	Na-P1 + Unknown
SC16	100	14.4	Na-P1
SC6	100	14.3	Na-P1 + K-A

Figure 6.12 shows the effect which temperature has on Si, Al and Na content in solution. The Si content at the start of the experiment is higher in the 75°C and one of the 100°C experiments, due to experimental error. The Si content by the end of the experiment has dropped in every case. For Al, it is uniform at the start of each experiment, and drops in all cases, but drops the most in the 100°C experiment. This indicates that there may still be yet-unconsumed Al in the soultion. The Na content drops in each case, but the largest drops are noted in the higher temeperature experiments.

The PSD graph shown in figure 6.13 shows that the largest particle sizes were produced at ambient temperatures, but the widest distribution was produced at 50°C, with a weighting towards the finer particle sizes. The 75°C and 100°C experiments are then of increasing size.

Hui et al (5) utilised a temperature step change (starting at 80°C - 95°C and then raising the temperature to 90°C or 95°C) in their crystallisation experiments in order to improve the purity of their yield and reduce energy consumed. This was done with the intent to halt the nucleation process with the increase in temperature, and induce crystallisation, resulting in improved crystallinity. As these experiments have only produced amorphous material at the lower temperatures, were the two-step method to be imple-

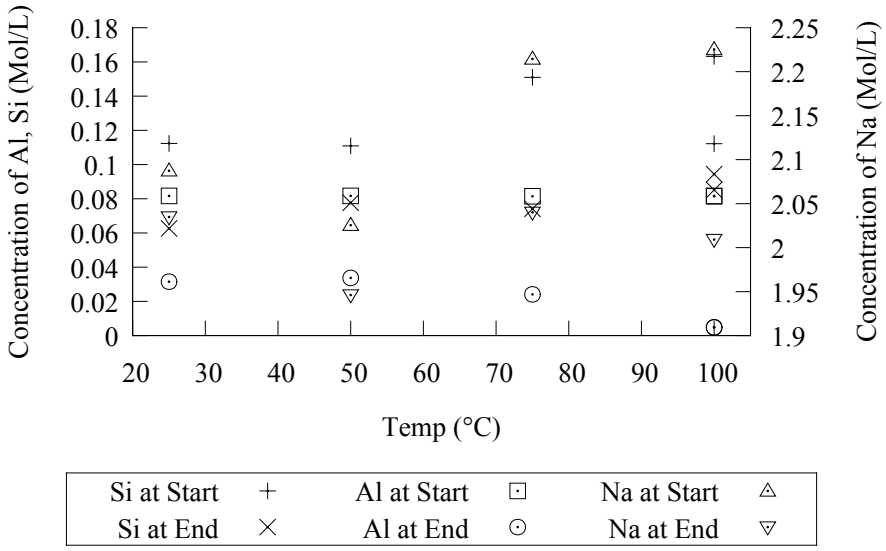

Figure 6.12: Effect of temperature of crystallisation step on Si, Al, and Na in solution

mented, temperatures of 75 °C or above should be utilised. However, due to the broad particle size in the SC17, this may indicate that nucleation and crystallisation were taking place simultaneously. Another option would be to seed the leachate at the start of the crystallisation step with zeolite already produced, as this has been shown to increase the speed of crystallisation (5).

6.4.7 Closed Loop System

In an industrial context, it is desirable to minimise effluent sent off for disposal, and the amount of NaOH consumed in the leaching process. Effluent sent for disposal will increase costs, especially if said effulents are highly caustic and contain heavy metals. It is desirable to minimise consumption of NaOH as this will further increase the cost of the process. The restults from the closed loop system are shown in table 6.5.

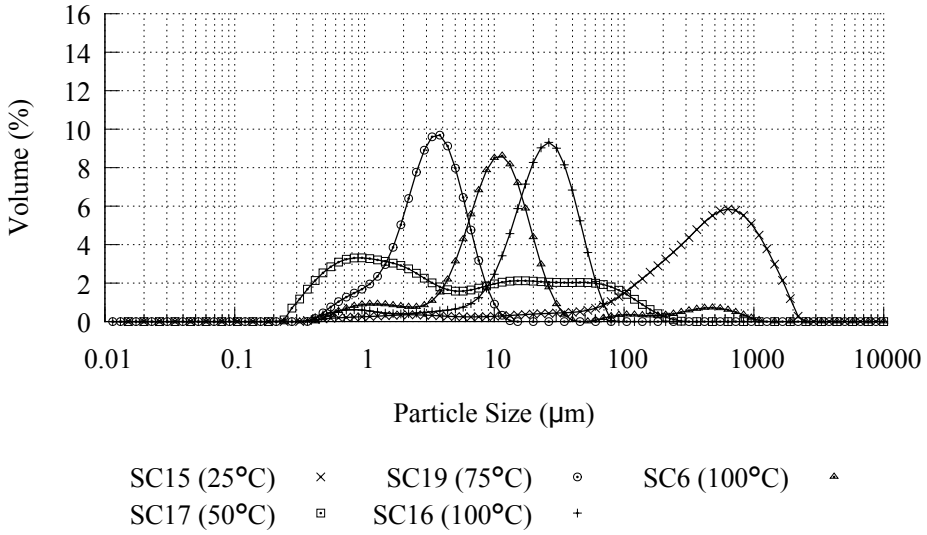

Figure 6.13: Effect of crystallisation temperature on particle size distribution

Table 6.5: Influence of recycling L2 in L1 on yield and form of zeolite

Experiment	Yeild (g)	Analysis
SC16	14.4	Na-P1
SC18	14.5	Na-P1
SC20	14.4	Na-P1
SC22	14.3	Na-P1 + Na-X

From this table, it is clear that the yield does not appear to be affected by the closed loop system. There appears to be some contamination with zeolite Na-X, but as can be seen from the XRD spectra in section 9, only trace amounts of Na-X are present, compared to the Na-P1.

Figure 6.14 shows the effects of recycling leachate on the Si, Al and Na content of the solutions over time. The most notable change is in the Al, which is fairly constant at the start of each experiment, but drops to a minimal amount by the end of each experiment. The starting concentration of Si in solution increases sharply after the first use, and continues to remain

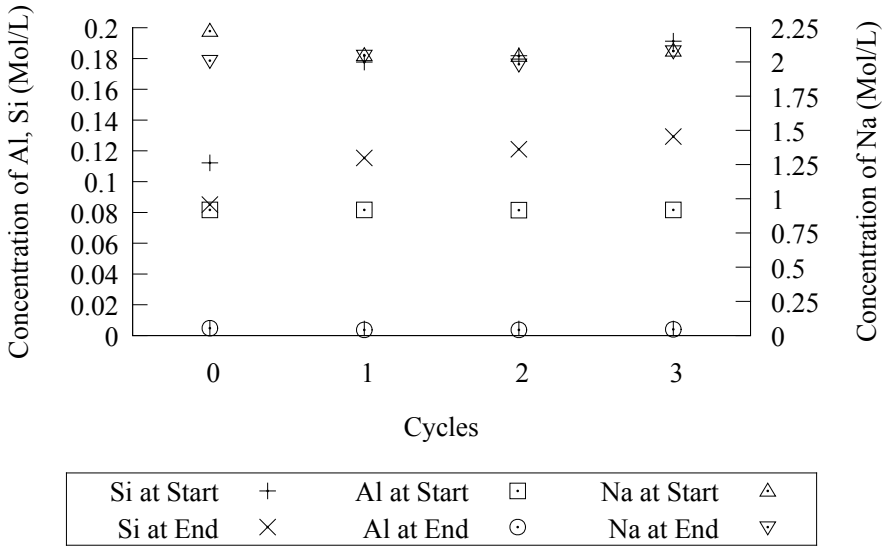

Figure 6.14: Effect of recycling leachate on Si, Al, and Na in solution

high thereafter. The Si left over at the end of each experiment rises with each recycling, which is consistent with what would be expected with incomplete consumption of Si in each experiment. The Na concentration seems to remain fairly constant betwen each cycle. The very low levels of Al in L2 and the left over Si does indicate that the Al content of the solution is the limiting factor in the reaction.

Figure 6.15 shows that the closed loop system has little to no effect on average particle size, or distribution of particle sizes, which is to be expected, as the temperature and time (being the factors theorised to be most influential in this system due to results shown in figures 6.11 and 6.13 were kept constant.

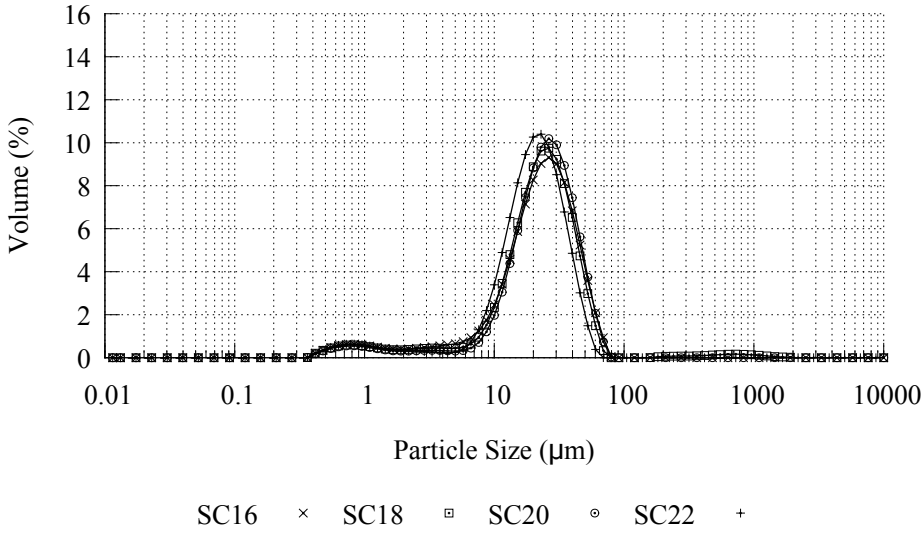

Figure 6.15: Effect of a closed loop system on particle size distribution

6.4.8 Floating Zeolites

Table 6.6 shows the effect of seeding the crystallisation solution with cenospheres. It is noted that the effect on yield does not appear to be high. It is also noted that mullite is one of the main components identified in the XRD of cenosphere samples, and thus is expected to be found in the XRD analysis of zeolitised cenospheres.

Table 6.6: Influence of cenosphere seeds on yield and form of zeolite

Exp	Seeds (g)	Yield (g)	Net Yield (g)	Analysis
SC21	12.5	25.7	13.2	Na-P1 + Mullite
SC23	25	37.7	12.7	Na-P1 + Mullite
SC24	50	61.4	11.4	Na-P1 + Mullite
SC28	100	115.6	15.6	Na-P1 + Mullite

The buoyancy of SC21, SC23 and SC24 was not noted as being particularly high during filtration. The volume of SC28 made it difficult to determine

the buoyancy of the sample during filtration. Preliminary analysis of SC24 through an optical microscope indicated that there was much more zeolite than cenosphere, which may account for the lack of buoyancy.

Figure 6.16 shows the effects which adding cenospheres to the crystallisation

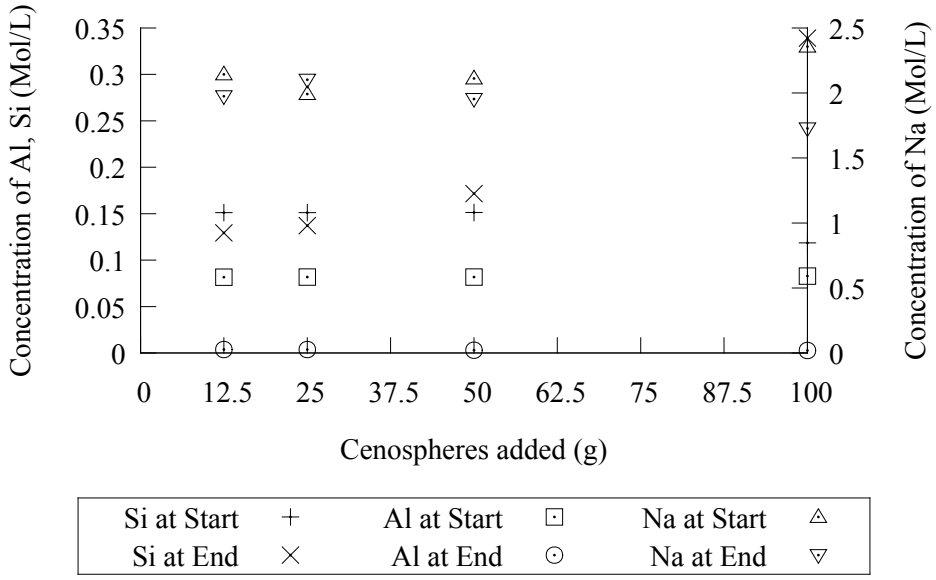

Figure 6.16: Effect of cenosphere seeding on Si, Al, and Na in solution

solution has on the concentrations of Si, Al and Na in solution. In every case, the Al content starts off relatively constant, and drops to a minimum by the end of the experiment. The Si content at the start is not as constant as the Al, but is all between 0.11M and 0.152M. The Si content at the end of the experiments drops slightly for the 12.5g and 25g experiments, increases slightly for the 50g experiment and increases significantly in the 100g experiment. The Na content drops in all experiments, except the 25g experiment, where it increases, which is put down to analytical error. The largest drop is in the 100g experiment, which correlates with the increase in Si content, indicating that Si was leached form the cenospheres into solution.

The PSD graphs shown in figure 6.17 show two distinct size peaks for

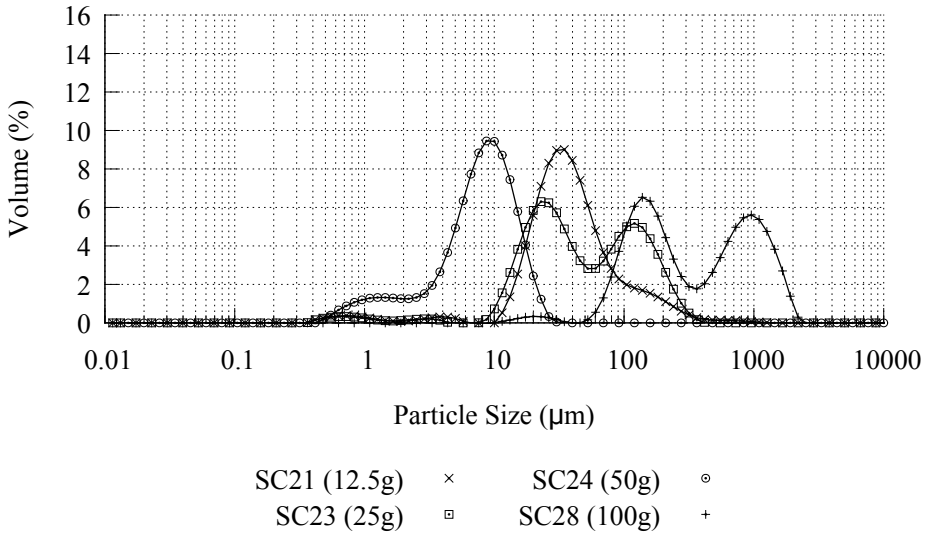

Figure 6.17: Effect of seeding with cenospheres on particle size distribution

the 100g and 25g seeded experiments, potentially due to separation between zeolite and cenospheres. The 12.5g seeded experiment shows an elongation towards the larger size range, but not a distinct peak, as with the 12.5g and 100g experiments. The 50g experiment shows an elongation towards the finer size range. It is noted that using water as the dispersion agent in the mastersizer is unlikely to provide an accurate measurement of the PSD for the floating zeolites, as the cenospheres are meant to float on water, thus will not be mixed, and measured by the mastersizer. Using a ligher medium such as alcohol may provide more accurate results. For this reason, these results are assumed to only measure the material which has low buoyancy.

6.4.9 Source Ash

Table 6.8 shows the effect source ash has on the yield and form of zeolite. SC16 uses alpha, the material most other experiments have utilised. The yield for FB7 is significantly higher than expected, however this may be put down to insufficient drying time for the zeolite produced. The yield for delta was higher than expected, at a similar level to that of alpha. Due to the lower surface area of the delta a lower yield of Si in solution and thus lower yield of zeolite was expected, but from the yields shown, the amount of zeolite produced does not appear to have been hindered. It is worth noting however, that the quantity of Si in solution is invariably higher than that of Al, therefore AAS analysis is required to determine the full effect of changing the source ash.

Table 6.7: Influence of source ash on yield and form of zeolite

Experiment	Ash	Yield (g)	Analysis
SC8	FB7	28.4	Na-P1
SC25	Delta	13.6	Na-P1
SC16	Alpha	14.4	Na-P1

Utilisation of delta as the feed source is desireable, as alpha already has other applications, and can already be sold on, but delta has fewer applications and is thus generally only sold as an aggregate, thus fetching a much lower price.

Figure 6.18 shows the effect which changing the source ash has on the elements on solution. The Si content falls in each case, except that of the delta, which may be down to an error in the AAS analysis of L2, which was

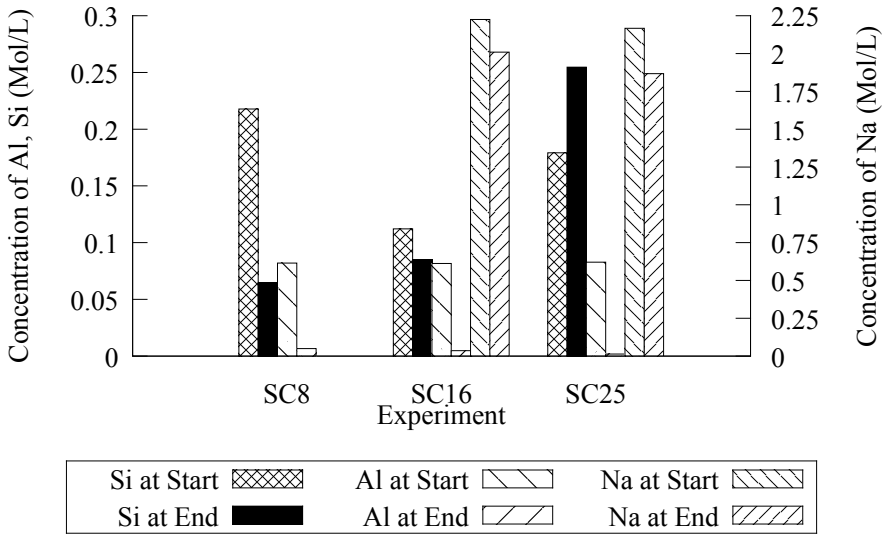

Figure 6.18: Effect of source ash on Si, Al, and Na in solution

abnormally high, or leaching of Si from the glassware. The Al is consumed, as expected, in every experiment, leaving minimal amounts by the end of the experiment. The Na content decreases for the alpha and delta, and but Na content was not measured for the the FB7 leaching experiment, as Na measurements started from experiment SC10.

Figure 6.19 shows the influence changing the source ash has on the particle size distribution. From this data, it would appear the alpha product produces larger particles, delta produces finer particles, and untreated ash produces a mixture of fine and large particles with more large particles than small particles. This may be due to untreated ash containing a higher proportion of fine particles (which form the majority of the alpha product) than coarse particles (which forms the majority of the delta product). The difference between particle sizes was not expected. The difference may be explained by the alpha product's leachate containing particles small enough to pass

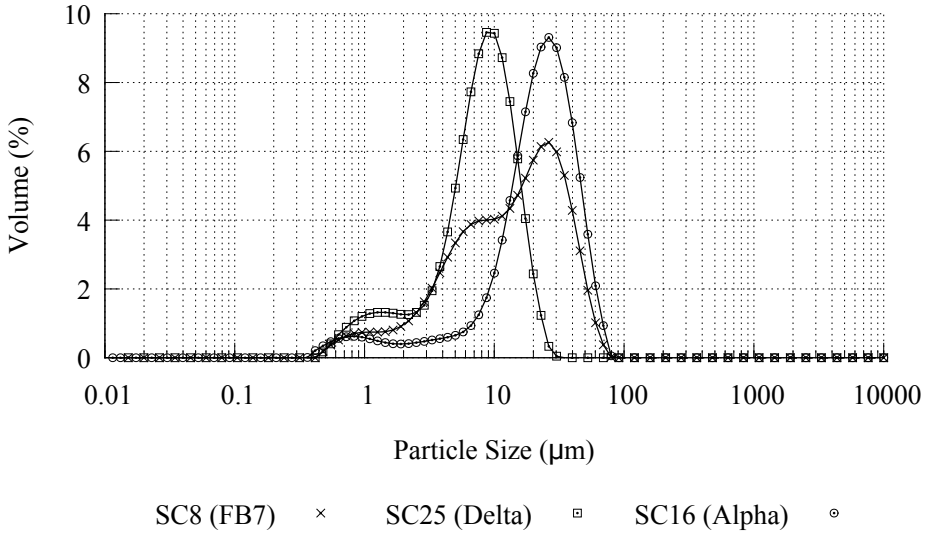

Figure 6.19: Effect of source ash on particle size distribution

through the filter. These particles may act as seeds for the crystallisation process, producting larger crystals than the delta leachate, which may spend the first part of the crystallisation process undergoing nucleation, before crystal growth can occur.

6.4.10 Highly Caustic Leaching

Table 6.8: Influence of leaching at 8M NaOH on yield and form of zeolite

Exp	Ash	SA (g)	L2 Conc (%)	Yeild (g)	Eff. Yield (g)	Analysis
SC2	Alpha	1.65	100	3.28	1.929	Sodalite
SC9	Alpha	8	25	10.9	21.8	ZK-14 + LTA
SC27	Alpha	4	25	6	12	Na-P1 + Na-A
SC26	Delta	4	25	6.3	12.6	Na-P1 + K-A

Table 6.8 shows the effect that using 8M NaOH in the leaching step has on yield and form of zeolite at various SA additions, and dilutions of L1 in

L2. SC2 was mentioned in a previous section, in that L1 was not diluted and it produced sodalite. The low yield is due to the low addition of SA, at only 1.65g. The effective yeild shows how much zeolite would have been produced, were 500ml of L1 used to make the crystallisation solution for L2. In the case of SC2, where 100% of the leachate was used, as around 850ml of L1 were produced, the yield of 3.28g was multiplied by (500ml/850ml). In all other cases, the yield was doubled, to account for using 500ml of L1 in the crystallisation step, rather than 250ml. Experiments SC9 and SC27 are effectively the same, except for the time of filtration and dosing of SA mentioned earlier. SC9 has a higher yield, but this is proportional to the higher dosage of SA. SC9 produced a mixture of zeolite ZK-14 (or sodalite - see section 6.5.2) and LTA. Experiments SC27 and SC26 are the same but for the source ash. SC26 has a slightly higher yield than SC27, again indicating that delta is a viable source material for leaching. Both produce zeolite Na-P1 and zeolite A. Figure 6.20 shows the effect of using 8M NaOH in the leaching step. No AAS data is available for SC2. The first difference to note is that the Al consumption does not appear to be as complete with these conditions as with others. This could be due to the proportion of Si in solution being lower, due to the higher dilution, making it appear as though less Al is consumed. The final Al values are still comparible to other conditions. The Si values drop as expected, with the drop in Si content being very similar for SC26 and SC27, which is to be expected due to the same experimental conditions. It is noted that there is very little change in the Na content for both SC26 and SC27, which is not unexpected when compared to the other experiments.

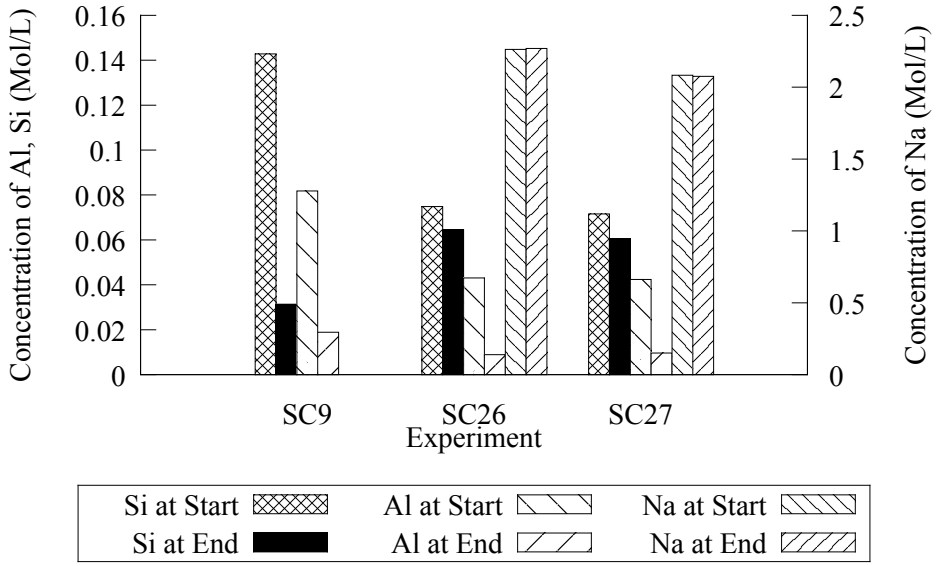

Figure 6.20: Effect of 8M leaching on Si, Al, and Na in solution

Figure 6.21 shows the difference between the PSD from various 8M leaching

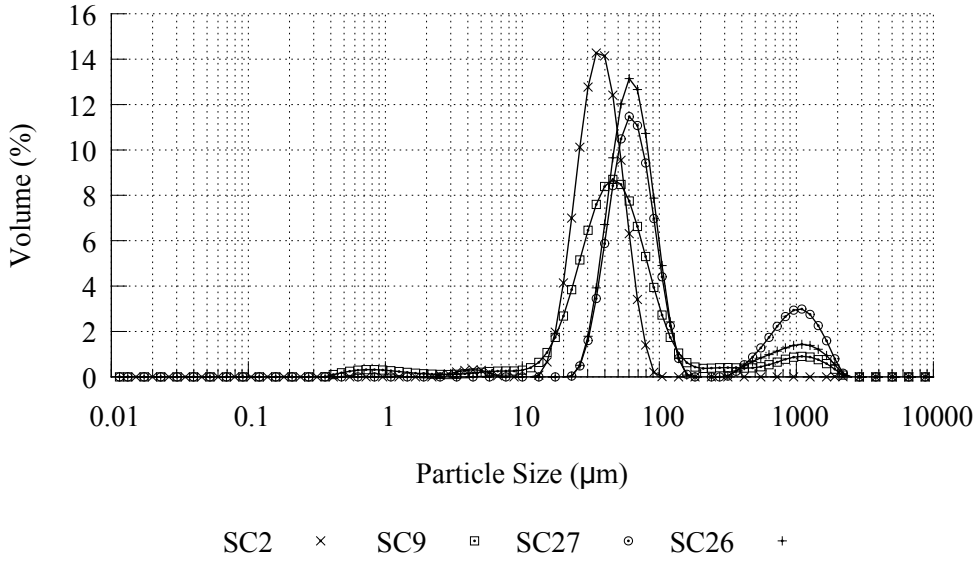

Figure 6.21: Effect of source ash on particle size distribution

experiments. As shown, the PSD's are quite similar, with fairly narrow size

distributions, and occasionally a tail of larger sized crystals.

6.4.11 Other Experiments

Experiment SC29, with gradual addition of SA in 5g aliquots produced a 12.7g yield of zeolite Na-A with sodalite (see section 9). It was expected that a higher yield of zeolite would be produced, owing to the higher dosage of SA added to the crystallisation, but the lower yield could be due to several factors. The vessel containing the SA solution prepared at the start of the 12h experiment had insoluble precipitate (presumably alumina) precipitated on the inside by the end of the experiment. This indicates that the entirety of the 20g of SA which was to be administered was not administered (as it remained precipitated inside the SA vessel), thus explaining the potentially lower yield. Additionally it was observed that the precipitate formed mainly on the inside surface of the vessel, and this deposit could only be removed with the assistance of the tip of a metal spatula. This is the only case in which such a crystallisation on the inside of the vessel was observed, but it is possible that this influenced the crystallisation process. The zeolite produced is the same as the zeolite produced last time a large quantity of SA was added to solution (SC7: 16g). It should be noted that the XRD spectra of zeolite ZK-14 and sodalite are both exceedingly similar (see section 6.5.2), hence the conclusion that the products may be the same.

Figure 6.22 shows the effects of repeated addition of SA. From this figure it is clear that almost all of the Si has been consumed. Whilst the Si has been consumed, Al is left in solution, indicating that excess Al was added.

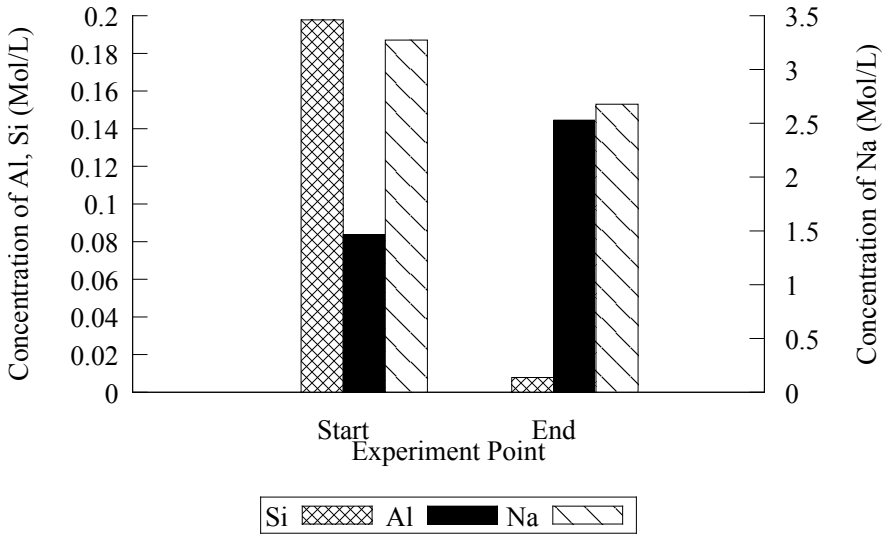

Figure 6.22: Effect of repeated addition of Al on Si, Al, and Na in solution

The Na content has reduced, as per usual. The PSD is shown in figure 6.23. The PSD shows two distinct peaks for two particle sizes, this may be due to one set of particles or phrase of zeolite nucleating and growing until all available resources are consumed, and then another form of zeolite forming when further SA was added to the solution.

In experiment SC30, concentrated sulphuric acid was added to the solution in order to neutralise some of the NaOH and reduce waste in a closed loop system. The experiment produced a yield of 15.6g of sodalite. This may indicate that pH does not have as much influence on the type of zeolite produced as was first thought from the dilution experiments. It may be that the Na content is the deciding factor. It should be noted that when the sulphuric acid was added, due to the heat evolved from the neutralisation reaction, a fizzing noise and vapour were observed upon the addition of each drop of acid. This may indicate that some of the acid evapourated and not

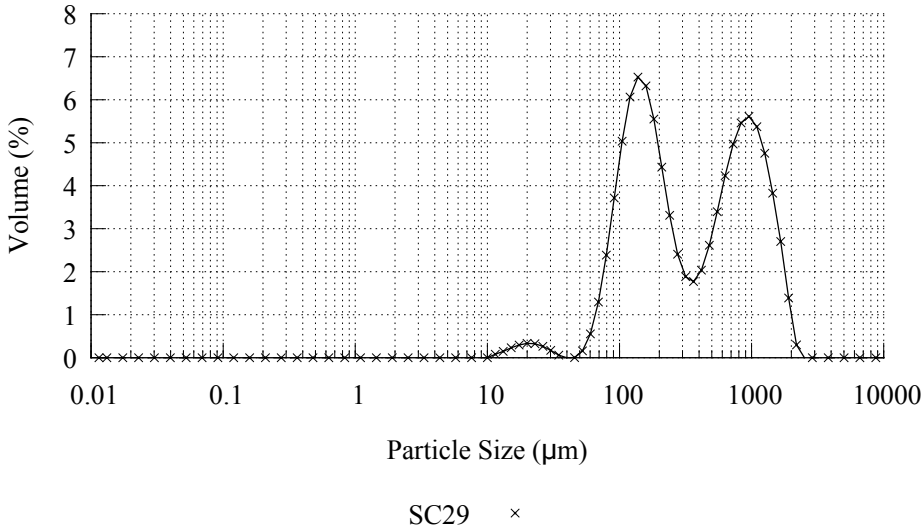

Figure 6.23: Effect of source ash on particle size distribution

all of the acid was added to the solution.

Figure 6.24 shows the effect which the addition of sulphuric acid has on the Si, Al and Na content. The figure indicates that although the Si content has reduced a bit by the end of the experiment, the Al has run out, indicating that more Al could be added to increase the yield. There appears to only be a minimal change in the Na content. Figure 6.25 shows the PSD from SC30. It shows one peak, with some some finer particles. The distribution is fairly wide, potentially indicating that nucleation and crystallisation were concurrent throughout the experiment.

6.4.12 Strategic Metals

Throughout the crystallisation experiments, various samples were analysed for Ge and Ga content. Experiments SC6 (benchmark) SC16, SC18, SC20 and SC22 (recycle experiments) and SC21 (5 minute filtration) were analysed

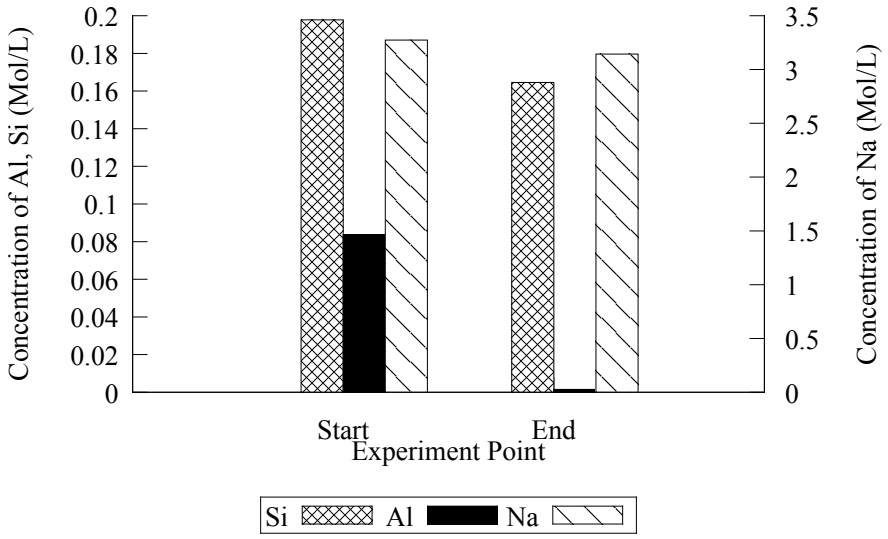

Figure 6.24: Effect of neustralisation on Si, Al, and Na in solution

for Ga and Ge content.

Figure 6.26 shows the Ga and Ge contents for various experiments. SC6 has a surprising increase in Ga content between L1 and L2. This is surprising because L1 is diluted to form L2, and no addional ash is present in the crystallisation step, thus the increase of Ga is unexpected. The parity in values between L1 and L2 for experiments SC16 and SC22 is also surprising. It is expected that L2 will be half L1, due to the dilution. The AAS results should be accurate to within 100ppb, thus any discrepancy is unlikely to be due to analytical error. The net increase in Ga between SC16, SC18, SC20 and SC22 is promising. Were a closed loop system to be implemented for the leaching process, it may be possible for the leachate to be sold for Ga and Ge extraction after several cycles if a closed loop system without any dilution were developed. The Ge content in L1 increases from just under 1mg/l to 2mg/l by SC22. With the exception of SC20 and SC21, where

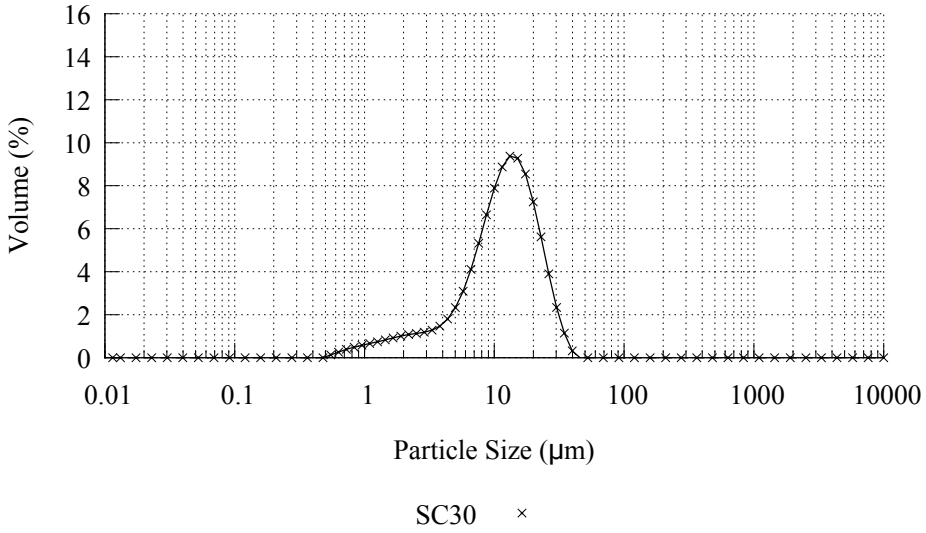

Figure 6.25: Effect of source ash on particle size distribution

similar levels of Ge are observed in both L1 and L2, L2 is lower than L1, as would be expected due to dilution. The Ga content also increases between cycles, but not to as great an extent. The extraction yields were not as high as those predicted in the literature (18; 19). This is likely due to the difference in conditions. In the literature cited Ge extraction was conducted using distilled water and Ga extraction was conducted using 0.7-1M NaOH. The differences in conditions, combined with fewer recirculation cycles are likely to have had a significant influence.

6.4.13 Starting Conditions for given Zeolites

In an attempt to predict which zeolites will be formed at any given condition, the ratios of Si, Al and Na to water were plotted in figure 6.27, however no obvious trend was observed. This could be due to accurate AAS analysis of Si being relatively difficult. It was hoped that there would be an observable

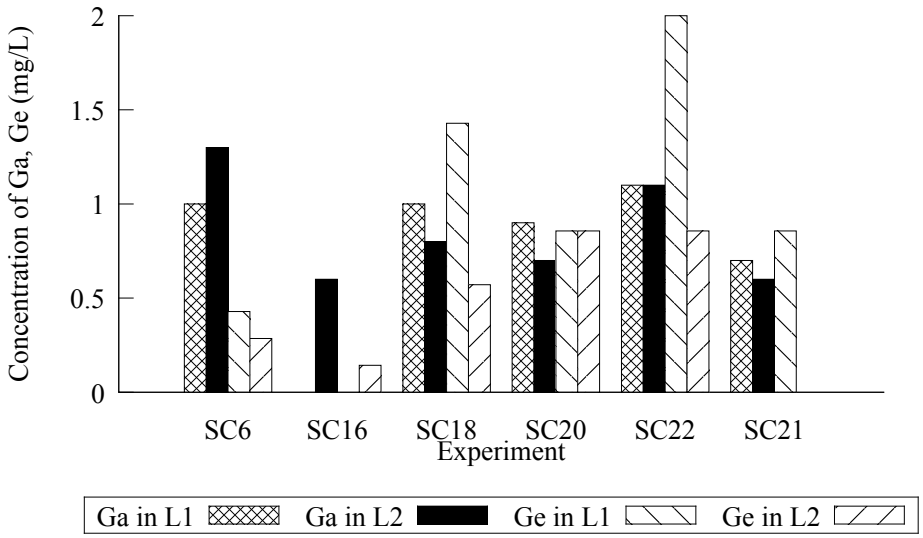

Figure 6.26: Ga & Ge content in various experiments

difference between experiments SC8-28 which produced zeolite Na-P1, SC0 & SC30 which produced Sodalite, and SC4, 6, 13 and 26, which produced a mixture of zeolite Na-P1, and zeolite A. If the sulphuric acid added in SC30 did not properly mix with the leachate, it is possible that pH may still be a deciding factor in zeolite crystallisation, thus pH measurements may help in the prediction of which zeolite will be formed from the leachate.

6.5 Synthesised Zeolites

6.5.1 XRF Analysis

XRF analysis was conducted on the first few crystallised samples. A comparison of the Si, Al and Na content of 7 experiments is shown in figure 6.28. Only Si, Al and Na are shown in this graph, as they are the elements most of interest. The main purpose of the XRF analysis was to identify what

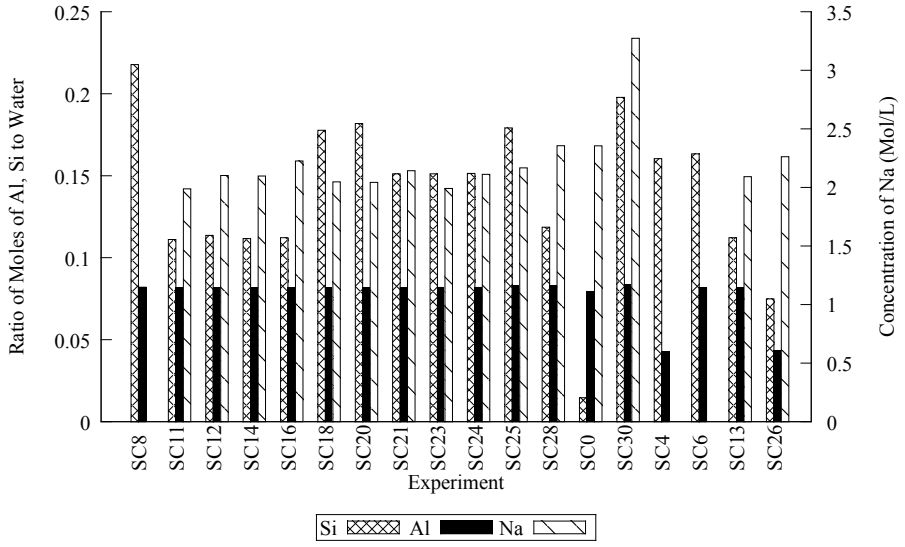

Figure 6.27: Starting conditions for various zeolites produced

the main elemental components of the samples were in order to make XRD analysis faster. The data could also be used to confirm what the products of crystalisation were.

6.5.2 XRD Analysis

Figure 9.1 on page 97 shows XRD spectra from experiments SC0, SC1, SC2, SC30 and zeolitised ash. With the exception of the ash, they all contain high purity sodalite. It is noted that the peaks for zeolite ZK-14 and sodalite are quite similar, making differentiation between the two quite difficult. References to zeolite ZK-14 in literature are rare. In some cases zeolite ZK-14 appears to produce a slightly better fit to the XRD pattern than sodalite (in that the peaks measured are closer to the example spectra on the 2-Theta axis), thus has been utilised, however sodalite also fits, therefore in cases where disagreements with literature arise, it may be preferable to assume

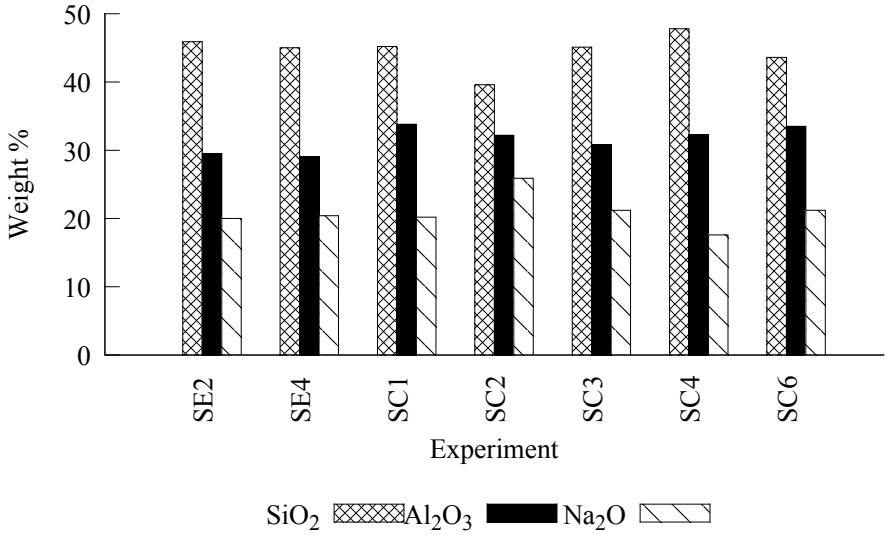

Figure 6.28: XRF analysis of precipitates

that references to ZK-14 in this thesis refer to sodalite. Figure 9.2 shows XRD spectra from Experiments SE2, SE4, SC8, SC11, SC12, SC14, SC16, SC18, SC20 and SC25, which all contain high purity zeolite Na-P1. Figure 9.3 shows XRD spectra from the cenosphere seeded experiments: SC21, SC23, SC24 and SC28. These all show high concentrations of Na-P1, but also contain mullite, a phase commonly found in cenospheres. Figure 9.4 shows XRD spectra from experiments SC4, SC6, SC13 and SC26 which produced zeolite Na-P1 and K-A. Figure 9.5 shows experiments SC7, SC9, SC10, SC27 and SC29, which all contain zeolite Na-A or LTA. These come mixed with zeolite Na-P1, and sodalite/ zeolite ZK-14. Figure 9.6 shows experiments SC3, SC19 and SC22, which contain Na-X or unidentified phases mixed with zeolite Na-P1. Experiments SC15 and SC17, were the low temperature experiments which produced amorphous material and are not shown. For all samples, determination of the precise purity of mixed samples proved difficult

due to the number of phases present.

6.5.3 Comparisons with Literature

Yields generally appear to be quite good, when compared to results produced by Hollman et al (32), who produced yields of between 50g and 80g of zeolite per kg of fly ash, whereas most experiments in this thesis have produced yields of over 140g/kg CFA (see table 9.1), only using 500ml of the ˜850ml of L1 available for use. Hollman et al identified the zeolite produced as Na-P1. The XRD spectra for Na-P, Na-P1 and Na-P2 are very similar, thus it is entirely possible that the experiments conducted for this thesis have produced the same product. Hollman et al also produced Na-X and Na-A with sodalite, however reaction times were between 48 and 72 hours, rather than the 12 hour standard used in this thesis's experiments.

Jha et al (23) point out that extraction of Si from the ash will be influenced by the form the Si takes. Si in the glass phase will be more reactive than Si in the crystalline phase, thus Si extraction will vary, depending on the crystallinity of the ash presented.

6.5.4 Cation Exchange Capacity

After the absorption readings were attained for the Fe, Zn and Mn Standards, trendlines were added, and their formulae derived. The R^2 values for Fe and Mn respectively were 0.992 and 0.997 respectively. Due to the inconvenient shape of the Zn curve, but low spread in the values required, two trendlines were used for the zinc values covering four points. Using the

formulae from these trendlines, the metal content of the solutions at each absorbency reading was calculated. The same trendline approach was applied to the neutralisation with NaOH values. It is noted that the first five values for the Zn curve were significantly lower than the later values. The Zn content for untreated AMD for the neutralisation experiments was around 15ppm, wereas every other untreated minewater value thus far had a Zn content around 20ppm. The accuracy of the analysis should be +/- 1ppm. It is thus assumed that the zinc content in the the first batch (first five values) of samples is incorrect, and they are ignored. It is noted that the values were relatively linear, but ˜5ppm lower than anticipiated. This solves the problem of a sudden increase in zinc content part of the way through the neutralisation experiments. Figures 6.29 and 6.30 show the amounts of metal left in solution after the absorption experiments, and the amount of metal which should be soluble in the solutions at the given pH's.

In experiments with high loading of zeolite or zeolitised ash, the Fe is reduced to 0 within 2.5 minutes. Experiments with low loading of synthetic zeolite reduce the Fe content slightly, and zeolitised ash experiments increase the Fe content. Ash samples which have not been zeolitised increase the Fe content of the AMD at both high and low loading. Time appears to have only been influential for high loading unzeolitised ash, and low loading zeolitised ash, which saw an increase in Fe content of the synthetic AMD over time, indicating potential leaching of Fe from magnetite in the ash due to the acidic conditions.

More Zn is absorbed with the synthetic zeolite at higher loading than lower loading zeolitised and unzeolitised ash have similar amounts of zinc

absorbed at high and low solids loading. High loading zeolite Na-P1 has the most absorption of Zn, and appears to be the only one where time is influential. According to figure 6.29a, Zn absoption appears to be liner with respect to time, but it is noted that the time axis is logarithmic. It is also noted that the absorption of Zn was increasing up to the end of the experiment and does not yet appear to have reached steady state. It is possible that longer experiments may show yet higher absorption of Zn for high loading zeolite Na-P1.

The highest Mn absorption appears to take place in experiments with high loading of synthetic zeolite, with low loading of synthetic zeolite comparable to high loading of zeolitised ash, and low loading of zeolitised ash and high and low loadings of unzeolitised ash having a minimal impact on Mn content. The highest absorption of Mn appears to take place within 2.5 minutes of the start of the experiment for high loading of zeolite A and sodalite. Later samples exhibit a higher Mn content in solution, indicating re-absorption of Mn into solution. It is plausible that there is an interaction with Zn absorption, with Mn first being absorbed, and then Zn replacing it later.

With the exception of the Fe content, high loading of zeolite Na-P1 appears to be the most effective sample at removing absorbing metals from solution. The Fe still comes out of solution with zeolite Na-P1, however this is put down to the Fe precipitating out due to the increase in pH.

As an indication of approximate performance of the absorption materials, these experiments are deemed sufficient. For more detailed and reliable data, repeated neutralisation experiments to get a better idea of repeatability of the neutralisation data would be a priority. It may also be interesting to try

the experiment in a packed column system to mimic the utilsation of porous fabric or membranes filled with absorbent materials in a system of bunds to filter metals out of AMD for in-situ treatment. It may also be interesting to see the effect particle size has on the absorption and flow characteristics of AMD through any potential bund system. For this purpose, zeolitised delta may be of interest. Literature does note that absorprion of metals is improved given a higher pH, so it is unclear if much effort should be put into limiting the pH-changing effects of the addition of zeolite (26).

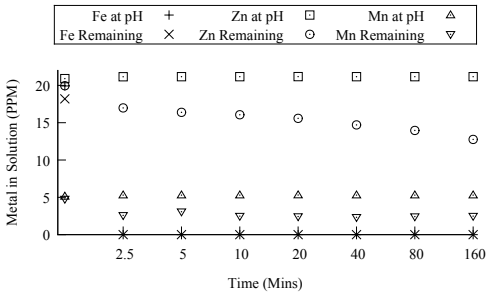

(a) Zeolite P: High Loading

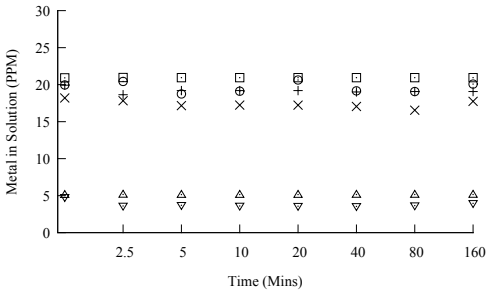

(b) Zeolite P: Low Loading

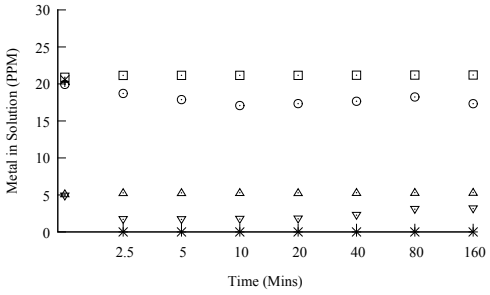

(c) Zeolite A: High Loading

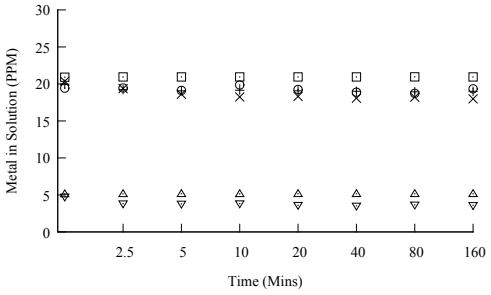

(d) Zeolite A: Low Loading

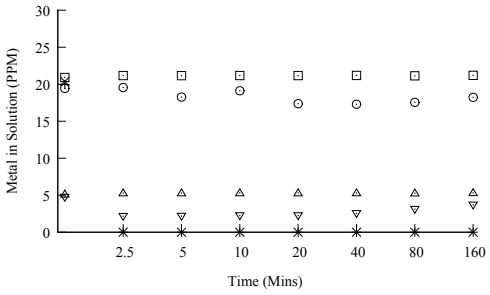

(e) Sodalite: High Loading

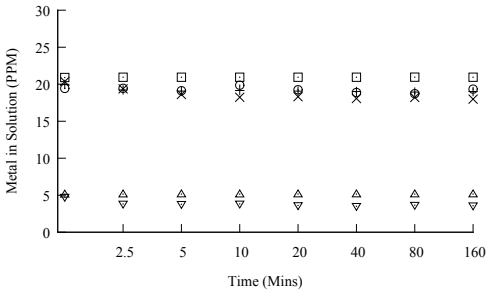

(f) Sodalite: Low Loading

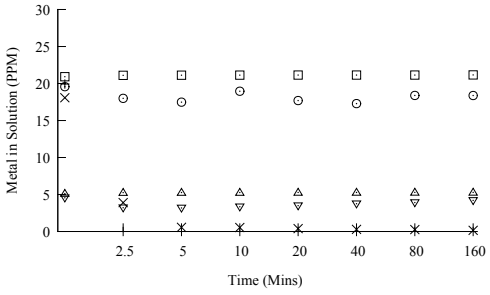

(g) 8M Zeolitised Ash: High Loading

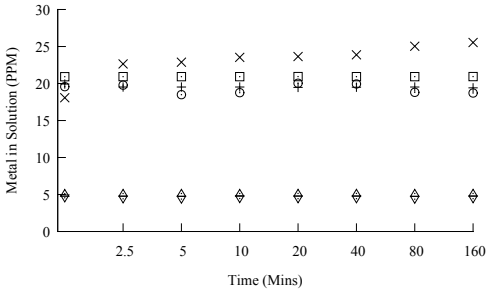

(h) 8M Zeolitised Ash: Low Loading

Figure 6.29: Cation exchange capacity tests

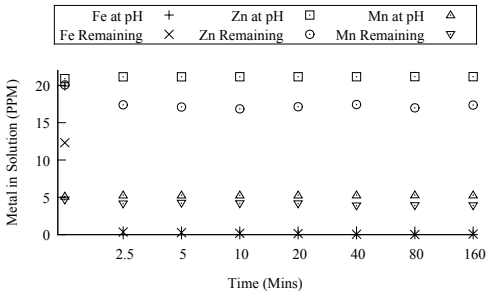

(a) 4M Zeolitised Ash: High Loading

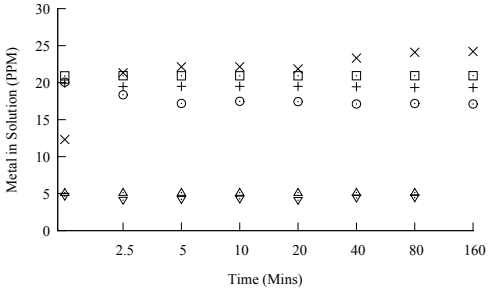

(b) 4M Zeolitised Ash: Low Loading

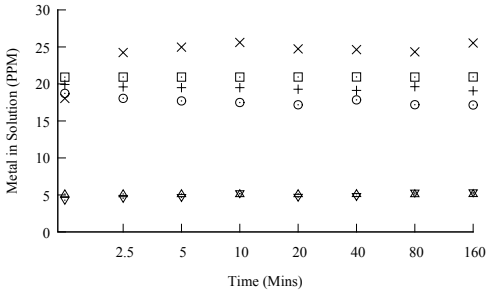

(c) Alpha: High Loading

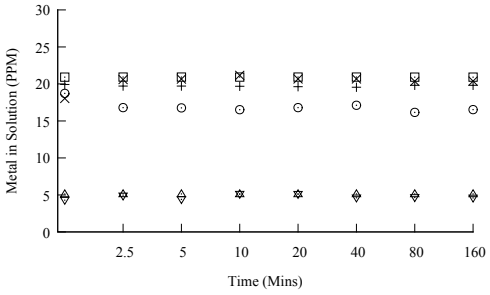

(d) Alpha: Low Loading

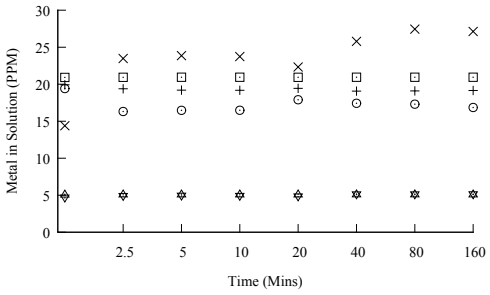

(e) Raw Ash: High Loading

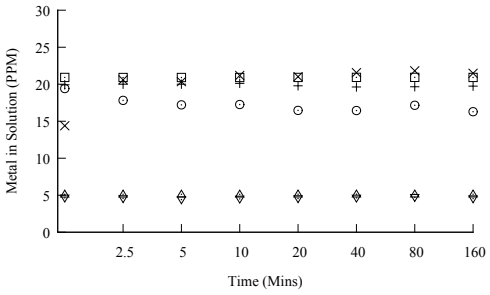

(f) Raw Ash: Low Loading

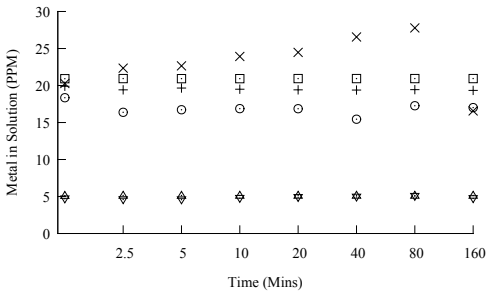

(g) Delta: High Loading

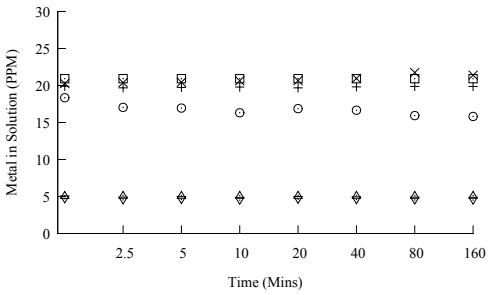

(h) Delta: Low Loading

Figure 6.30: Cation exchange capacity tests

Chapter 7

Conclusions

The zeolitisation of coal fly ash is influenced by many factors. Highest yields of Si in solution were found at 100g of fly ash per litre of NaOH at 4M or possibly even 8M under reflux. In order to avoid precipitating sodalite, it is necessary to dilue the leachate. Dilution by 50% proved effective and produced high yeilds of zeolite Na-P1. The highest yeilds of zeolite Na-P1 were found by adding 8g of sodium aluminate to the crystallisation solution. In order to achieve good repeatability it is necessary to control the time between the end of the experiment and the separation of leachate and ash. Longer crystallisation steps were found to produce higher yields of zeolite with larger crystal sizes, with diminishing returns after 12 hours. Crystallisation of zeolite at lower temperatures tended to produce lower yields of material, which after analysis was found to be amorphous. A partially closed loop system was shown to have minimal effect on the yield or purity of zeolite, indicating that a closed loop system could be achieved were the problem of dilution to be overcome. The products formed from the crystallisation steps were

tested for absorption of metals from synthetic acid mine drainage, however it is unclear if the reduction in metal content is due to cation exchange of the zeolite, or the effects the zeolite has on pH of the AMD. Utilisation of zeolites for remediation of AMD is preferable to dumping of NaOH in order to change the pH of the water system, as pH control requires close montoring. Overdosing of NaOH will also have adverse effects on the environment. In comparison, overdose of zeolite should be harmless, thus zeolite provides a good example of a passive remediation system well adapted for polishing AMD effluents, as mentioned by Moreno et al (30).

Chapter 8

Further Work

There is much scope for further work, including but not limited to the following fields:

8.1 Effects of pH

- Utilising titration experiments to more accurately measure the pH of L1 prior to crystallisation for a more controlled method in order to better predict zeolites formed.
- Neutralising the pH of L1 with acid, and then re-checking the pH prior to crystallisation.
- As NaOH is utilised to regulate alkalinity, testing the influence of the Na at constant pH, to ascertain if the influence of NaOH content is due to the alkalinity, Na content, or both. This could be achieved through the addition of salts, but ideally not, as it is noted that halide salts already influence the reaction (24; 23).

8.2 Seeding

- Investigate by how much addition of halide salts will increase yield, as mentioned by Barrer et al (24), and Jha et al (23). An improvement in crystallinity, shortening of nucleation period and improvement in the CEC of the synthesised zeolite is anticipated through the addition of NaCl, with a greater improvement when utilising NaF.
- Improved growth of zeolites utilising zeolite as seeds, crystallisation agents to speed up the process, and structure directing agents such as CTAB in order to direct which zeolite is produced.

8.3 Floating Catalysts

- Sink/float tests, and CEC tests for the floating zeolites produced in these experiments.
- Utilising a higher concentration of cenospheres in the production of floating cenospheres.
- Utilising cenospheres with a higher buoyancy through density separation with ethanol or another lower density medium. The higher buoyancy is intended to produce floating catalysts with better buoyancy.
- Utilising Fe^3+ to shift the absorption edge of TiO_2 into the visible light spectrum and coating onto cenospheres to produce a floating catalyst as demonstrated by Wang et al (45; 46).
- Acid treatment of zeolite to reduce the effects of zeolite on pH.

8.4 Further analysis

- Further experiments on zeolitisation of untreated fly ash to address unexpected results from this thesis, and to ascertain the influence of different ashes on yield.
- Re-leaching of zeolitised ash.
- Investigate the reason for the as yet unexplained orange-brown colouring of L1.
- Continuous process leaching, where NaOH is raised to boiling temperature and passed through a Büchner funnel full of ash for quick extraction of Si & Al on ash without the zeolitisation of the ash. The aim being to strip off glassy and amorphous materials before zeolite gets deposited producing a higher yield of Si in solution, as amorphous content makes up 34-80% of the material according to Vassilev et al (2).

8.5 Alternative methods of zeolitisation

- Microwave assisted hydrothermal leaching in order to reduce energy consumption as mentioned by Querol et al (31).
- Non-hydrothermal methods of zeolite synthesis, such as direct sintering of ash with NaOH.

8.6 Multicomponent utilisation and new products

- Multicomponent reutilisation of fly ash with the production of a paralell channel monolith of zeolitised delta, washcoated with synthetic zeolite for applications where a low pressure drop is required.
- Precipitation of silica-rich hollowspheres on sacrificial cores.

References

[1] X. Querol, "Synthesis of zeolites from coal fly ash: an overview," *International Journal of Coal Geology*, vol. 50, pp. 413–423, May 2002.

[2] S. V. Vassilev and C. G. Vassileva, "Methods for characterization of composition of fly ashes from coal-fired power stations: a critical overview," *Energy & Fuels*, vol. 19, pp. 1084–1098, May 2005.

[3] R. Blissett and N. Rowson, "A review of the multi-component utilisation of coal fly ash," *Fuel*, vol. 97, pp. 1–23, July 2012.

[4] M. Ahmaruzzaman, "A review on the utilization of fly ash," *Progress in Energy and Combustion Science*, vol. 36, pp. 327–363, June 2010.

[5] K. Hui and C. Chao, "Effects of step-change of synthesis temperature on synthesis of zeolite 4A from coal fly ash," *Microporous and Mesoporous Materials*, vol. 88, pp. 145–151, Jan. 2006.

[6] R. Iyer and J. Scott, "Power station fly ash a review of value-added utilization outside of the construction industry," *Resources, Conservation and Recycling*, vol. 31, pp. 217–228, Mar. 2001.

[7] M. M. Maroto-Valer, D. N. Taulbee, and J. C. Hower, "Novel separation of the differing forms of unburned carbon present in fly ash using density gradient centrifugation," *Energy & Fuels*, vol. 13, pp. 947–953, July 1999.

[8] G. Ferraiolo, M. Zilli, and A. Converti, "Fly ash disposal and utilization," *Journal of Chemical Technology & Biotechnology*, vol. 47, pp. 281–305, Apr. 2007.

[9] N. Moreno, X. Querol, J. Andres, K. Stanton, M. Towler, H. Nugteren, M. Janssenjurkovicova, and R. Jones, "Physico -chemical characteristics of european pulverized coal combustion fly ashes," *Fuel*, vol. 84, pp. 1351–1363, Aug. 2005.

[10] N. Murayama, "Mechanism of zeolite synthesis from coal fly ash by alkali hydrothermal reaction," *International Journal of Mineral Processing*, vol. 64, pp. 1–17, Feb. 2002.

[11] H. Tanaka, "Formation of na-a and -x zeolites from waste solutions in conversion of coal fly ash to zeolites," *Materials Research Bulletin*, vol. 37, pp. 1873–1884, Sept. 2002.

[12] S. Ghosal, "Particle size-density relation and cenosphere content of coal fly ash," *Fuel*, vol. 74, pp. 522–529, Apr. 1995.

[13] J. A. Campbell, J. C. Laul, K. K. Nielson, and R. D. Smith, "Separation and chemical characterization of finely-sized fly-ash particles," *Analytical Chemistry*, vol. 50, pp. 1032–1040, July 1978.

[14] R. Sommerville, *Recycling Coal Fly Ash in the Manufacture of Useful Materials*. Research project, University of Birmingham, May 2011.

[15] S. P. McBride, A. Shukla, and A. Bose, "Processing and characterization of a lightweight concrete using cenospheres," *Journal of Materials Science*, vol. 37, pp. 4217–4225, 2002. 10.1023/A:1020056407402.

[16] S. Shukla, "Electroless copper coating of cenospheres using silver nitrate activator," *Materials Letters*, vol. 57, pp. 151–156, Nov. 2002.

[17] S. Vassilev, "Phase -mineral and chemical composition of coal fly ashes as a basis for their multicomponent utilization. 3. characterization of magnetic and char concentrates," *Fuel*, vol. 83, pp. 1563–1583, Aug. 2004.

[18] F. Arroyo and C. Fernndez-Pereira, "Hydro metallurgical recovery of germanium from coal gasification fly ash. solvent extraction method," *Industrial & Engineering Chemistry Research*, vol. 47, pp. 3186–3191, May 2008.

[19] O. Font, X. Querol, R. Juan, R. Casado, C. R. Ruiz, . Lpez-Soler, P. Coca, and F. G. Pea, "Recovery of gallium and vanadium from gasification fly ash," *Journal of Hazardous Materials*, vol. 139, pp. 413–423, Jan. 2007.

[20] F. Zheng, "Recovery of gallium from coal fly ash," *Hydrometallurgy*, vol. 41, pp. 187–200, June 1996.

[21] RockTron Ltd, "Fly ash beneficiation process & benefits-rktron.com." http://rktron.com/us-rocktron-fly-ash-beneficiation-process-benefits, 2011.

[22] T. Maesen and B. Marcus, "The zeolite sceneAn overview," in *Introduction to Zeolite Science and Practice* (H. V. Bekkum, J. Jansen, and E. Flanigen, eds.), vol. 137 of *Studies in Surface Science and Catalysis*, pp. 1 – 9, Elsevier, 2001.

[23] V. K. Jha, M. Matsuda, and M. Miyake, "Resource recovery from coal fly ash waste: an overview study," *Journal of the Ceramic Society of Japan*, vol. 116, no. 1350, pp. 167–175, 2008.

[24] R. M. Barrer, "Zeolites and their synthesis," *Zeolites*, vol. 1, pp. 130–140, Oct. 1981.

[25] B. Bonelli, B. Onida, B. Fubini, C. O. Aren, and E. Garrone, "Vibrational and thermodynamic study of the adsorption of carbon dioxide on the zeolite NaZSM-5," *Langmuir*, vol. 16, pp. 4976–4983, May 2000.

[26] K. Hui, C. Chao, and S. Kot, "Removal of mixed heavy metal ions in wastewater by zeolite 4A and residual products from recycled coal fly ash," *Journal of Hazardous Materials*, vol. 127, pp. 89–101, Dec. 2005.

[27] J.-S. Lee, J.-H. Kim, J.-T. Kim, J.-K. Suh, J.-M. Lee, and C.-H. Lee, "Adsorption equilibria of CO2 on zeolite 13X and zeolite x activated carbon composite," *Journal of Chemical & Engineering Data*, vol. 47, pp. 1237–1242, Sept. 2002.

[28] J. Mrel, M. Clausse, and F. Meunier, "Carbon dioxide capture by indirect thermal swing adsorption using 13X zeolite," *Environmental Progress*, vol. 25, pp. 327–333, Dec. 2006.

[29] A. Phan, C. J. Doonan, F. J. Uribe-Romo, C. B. Knobler, M. OKeeffe, and O. M. Yaghi, "Synthesis, structure, and carbon dioxide capture properties of zeolitic imidazolate frameworks," *Accounts of Chemical Research*, vol. 43, pp. 58–67, Jan. 2010.

[30] N. Moreno, X. Querol, C. Ayora, C. F. Pereira, and M. Janssen-Jurkovicov, "Utilization of zeolites synthesized from coal fly ash for the purification of acid mine waters," *Environmental Science & Technology*, vol. 35, pp. 3526–3534, Sept. 2001.

[31] X. Querol, J. C. Uma\ na, F. Plana, A. Alastuey, A. Lopez-Soler, A. Medinaceli, A. Valero, M. J. Domingo, and E. Garcia-Rojo, "Synthesis of na zeolites from fly ash in a pilot plant scale. examples of potential environmental applications," *Fuel*, vol. 80, no. 6, p. 857865, 2001.

[32] G. Hollman, "A two step process for the synthesis of zeolites from coal fly ash," *Fuel*, vol. 78, pp. 1225–1230, Aug. 1999.

[33] D. C. Harris, *Quantitative chemical analysis*. New York: W.H. Freeman and Co., 2003.

[34] B. Beckhoff, *Handbook of practical X-ray fluorescence analysis*. Berlin ;;New York :: Springer,, 2006.

[35] R. Stephenson, "XRF basic principles." http://stephenson-associates-inc.com/XRF%20Basic%20Principles.pdf, Mar. 2007.

[36] H. Saisho and H. Hashimoto, "Chapter 2 x-ray fluorescence analysis," in *Analytical Spectroscopy Library*, vol. 7, pp. 79–169, Elsevier, 1996.

[37] E. Villarreal, A. JordanValley, and xenemetrix.com, "Introduction to x-ray fluorescence analysis." www.learnxrf.com/powerpointpresentations/Basicxrf.ppt, Sept. 2002.

[38] P. Atkins and J. De Paula, *Elements of Physical Chemistry*. Oxford University Press, 4th ed., 2005.

[39] R. Schlotz and S. Uhling, *Introduction to X-Ray Fluorescence Analysis (XRF) User's Manual*. Bruker AXS GmbH, July 2004.

[40] P. Potts, "X-RAY FLUORESCENCE AND EMISSION | wavelength dispersive x-ray fluorescence," in *Encyclopedia of Analytical Science*, pp. 419–429, Elsevier, 2005.

[41] P. Atkins, T. Overton, J. Rourke, M. Weller, and F. Armstrong, *Inorganic Chemistry*. Oxford University Press, 4th ed., 2006.

[42] A. Chatterjee, "X-ray diffraction," in *Handbook of Analytical Techniques in Concrete Science and Technology*, pp. 275–332, Elsevier, 2001.

[43] I. Scintag, *Basics of X-ray Diffraction (Chapter 7)*. Scintag Inc, 1999.

[44] S. D. M. College, "Media to activities and experiments." http://faculty.sdmiramar.edu/fgarces/labmatters/instruments/aa/aa.htm, Apr. 2010.

[45] B. Wang, Q. Li, W. Wang, Y. Li, and J. Zhai, "Preparation and characterization of fe3+-doped TiO2 on fly ash cenospheres for photocatalytic application," *Applied Surface Science*, vol. 257, pp. 3473–3479, Feb. 2011.

[46] P. K. Surolia, R. J. Tayade, and R. V. Jasra, "TiO2 coated cenospheres as catalysts for photocatalytic degradation of methylene blue p-nitroaniline, n-decane, and n-tridecane under solar irradiation," *Industrial & Engineering Chemistry Research*, vol. 49, pp. 8908–8919, Oct. 2010.

Chapter 9

Appendix

Table 9.1: All crystallisation results

Variable	Ref	NaOH M	Si (g/l)	Al (g/l)	Na (g/l)	Al Add (g)	L1 used (%)	Temp C	Time (h)	Si (g/l)	Al (g/l)	Na (g/l)	Yeild (g) (g)	Pure	Analysis
Undiluted L2	SC1	4	—	—	—	20	100	100	12	—	—	—	31.68	x	Sodalite
8M, Undiluted L2	SC2	8	—	—	—	1.65	100	100	12	—	—	—	3.28	x	Sodalite
Al	SC3	4	—	—	—	1.6	50	100	12	—	—	—	1.9		Na-P1 + Unknown
Al	SC4	4	9.01	0.175	—	4	50	100	12	4.04	0.119	—	6		Na-P1 + K-A
	SC5	4	8.83	0.138	—	—	—	—	—	—	—	—	—		—
Al, Time, Temp	SC6	4	9.17	0.161	—	8	50	100	12	2.65	0.129	—	14.3		Na-P1 + K-A
Al	SC7	4	13.48	0.16	—	16	50	100	12	0.45	0.63	—	13.9		Na-A + ZK-14
Ash	SC8	4	12.23	0.19	—	8	50	100	12	1.81	0.18	—	28.4	x	Na-P1
8M	SC9	8	16.04	0.36	—	8	25	100	12	0.88	0.51	—	10.9		ZK-14 + LTA
Time	SC10	4	6.08	0.18	78.02	8	50	100	3	1.71	0.86	41.93	6.5		Na-P1 + LTA
Time	SC11	4	6.24	0.17	85.45	8	50	100	6	1.38	0.15	44.5	13.6	x	Na-P1
Time	SC12	4	6.38	0.17	90.7	8	50	100	48	—	—	—	14.2	x	Na-P1
Time	SC13	4	6.3	0.16	90.23	8	50	100	24	2.63	0.12	46.01	14.5		Na-P1 + K-A
Time	SC14	4	6.27	0.17	90.51	8	50	100	48	4.8	0.09	46.01	15	x	Na-P1
Temp	SC15	4	6.31	0.17	90.05	8	50	25	12	1.76	0.85	46.78	8.4		Amorphous
Recycle	SC16	4	6.3	0.17	96.39	8	50	100	12	2.39	0.13	46.19	14.4	x	Na-P1
Temp	SC17	4	6.23	0.17	87.2	8	50	50	12	2.18	0.91	44.74	9.1		Amorphous
Recycle	SC18	4	9.98	0.17	88.21	8	50	100	12	3.24	0.1	47.06	14.5	x	Na-P1
Temp	SC19	4	8.48	0.16	95.89	8	50	75	12	2.08	0.65	46.9	8.2		Na-P1 + Unknown
Recycle	SC20	4	10.21	0.16	87.99	8	50	100	12	3.4	0.1	45.58	14.4	x	Na-P1
Seeds (HF)	SC21	4	8.49	0.17	92.61	8	50	100	12	3.63	0.1	45.41	25.7	?	Na-P1 + Mullite
Recycle	SC22	4	10.74	0.17	89.74	8	50	100	12	3.63	0.11	47.8	14.3		Na-P1 + Na-X
Seeds (HF)	SC23	4	8.49	0.18	85.64	8	50	100	12	3.85	0.1	48.33	37.7	?	Na-P1 + Mullite
Seeds (HF)	SC24	4	8.5	0.18	91.16	8	50	100	12	4.82	0.08	44.93	61.4	?	Na-P1 + Mullite
Ash	SC25	4	10.06	0.23	93.7	8	50	100	12	7.15	0.05	42.93	13.6	x	Na-P1
8M, Ash	SC26	8	8.41	0.41	202.15	4	25	100	12	1.81	0.24	52.17	6.3		Na-P1 + K-A
8M	SC27	8	8.04	0.34	185.6	4	25	100	12	1.7	0.26	47.71	6		Na-P1 + Na-A
Seeds	SC28	4	6.66	0.23	102.42	8	50	100	12	9.52	0.07	39.73	115.6	?	Na-P1 + Mullite
Slow Addition	SC29	4	3.77	0.32	108.26	20	50	100	12	0.22	3.9	61.55	12.7		Na-A + Sodalite
Undiluted L2	SC30	4	7.12	0.18	92.67	8	100	100	12	4.62	0.04	72.26	15.6	x	Sodalite
Blank	SC0	4	0.82	0.05	102.37	8	50	100	12	0.6	2	58.42	1.2	x	Sodalite

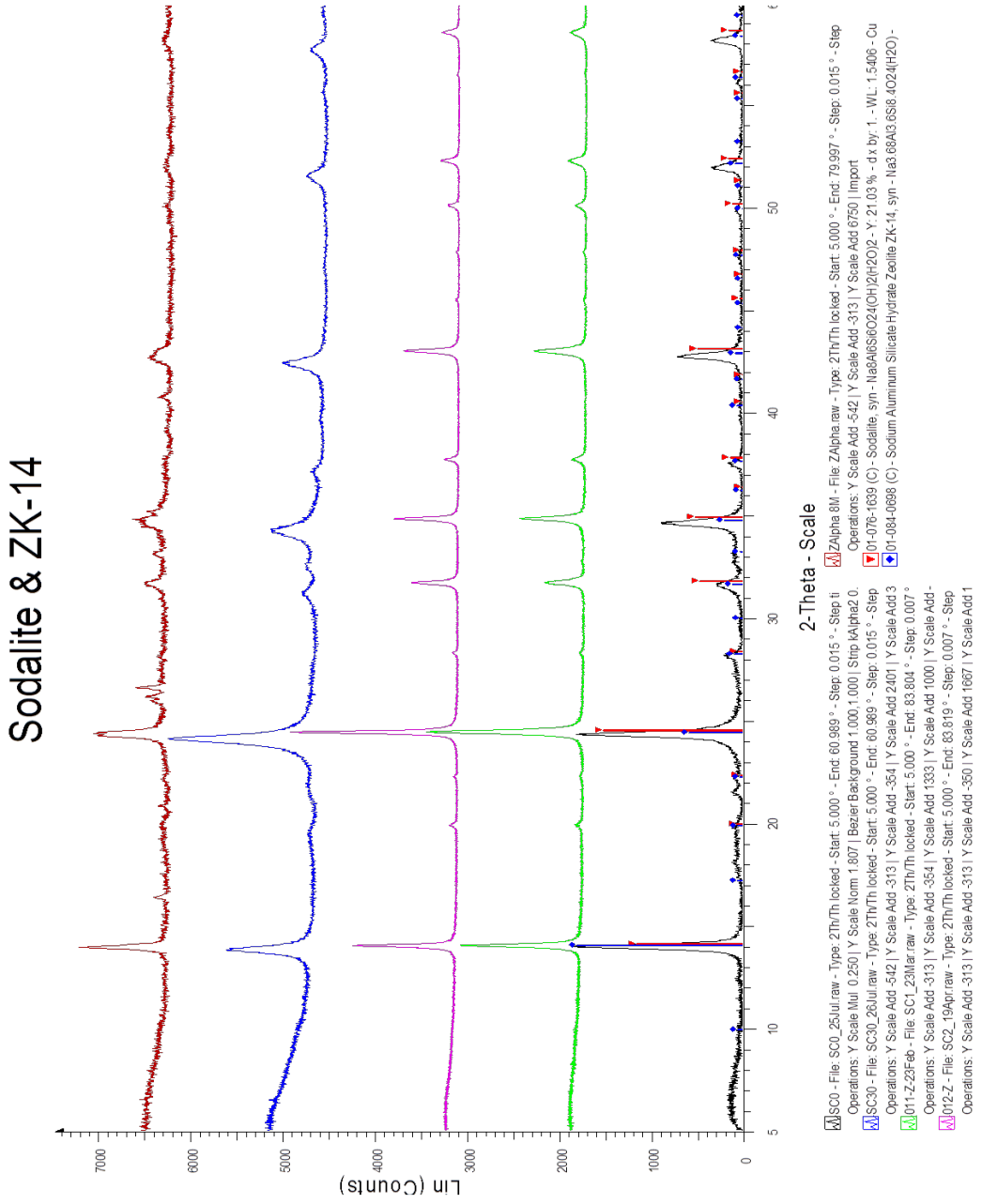
Sodalite & ZK-14
Lin (Counts)
2-Theta - Scale
SC0 - File: SC0_25Jul.raw - Type: 2Th/Th locked - Start: 5.000 ° - End: 60.969 ° - Step: 0.015 ° - Step ti
Operations: Y Scale Mul 0.250 | Y Scale Norm 1.807 | Bezier Background 1.000,1.000 | Strip kAlpha2 0.
SC30 - File: SC30_26Jul.raw - Type: 2Th/Th locked - Start: 5.000 ° - End: 60.969 ° - Step: 0.015 ° - Step
Operations: Y Scale Add -542 | Y Scale Add -313 | Y Scale Add -354 | Y Scale Add 2401 | Y Scale Add 3
011-Z-23Feb - File: SC1_23Mar.raw - Type: 2Th/Th locked - Start: 5.000 ° - End: 83.804 ° - Step: 0.007 °
Operations: Y Scale Add -313 | Y Scale Add -354 | Y Scale Add 1333 | Y Scale Add 1000 | Y Scale Add -
012-Z - File: SC2_19Apr.raw - Type: 2Th/Th locked - Start: 5.000 ° - End: 83.819 ° - Step: 0.007 ° - Step
Operations: Y Scale Add -313 | Y Scale Add -350 | Y Scale Add 1667 | Y Scale Add 1
ZAlpha 8M - File: ZAlpha.raw - Type: 2Th/Th locked - Start: 5.000 ° - End: 79.997 ° - Step: 0.015 ° - Step
Operations: Y Scale Add -542 | Y Scale Add -313 | Y Scale Add 6750 | Import
01-076-1639 (C) - Sodalite, syn - Na8Al6Si6O24(OH)2(H2O)2 - Y: 21.03 % - d x by: 1. - WL: 1.5406 - Cu
01-084-0698 (C) - Sodium Aluminum Silicate Hydrate Zeolite ZK-14, syn - Na3.68Al3.6Si8.4O24(H2O) -

Figure 9.1

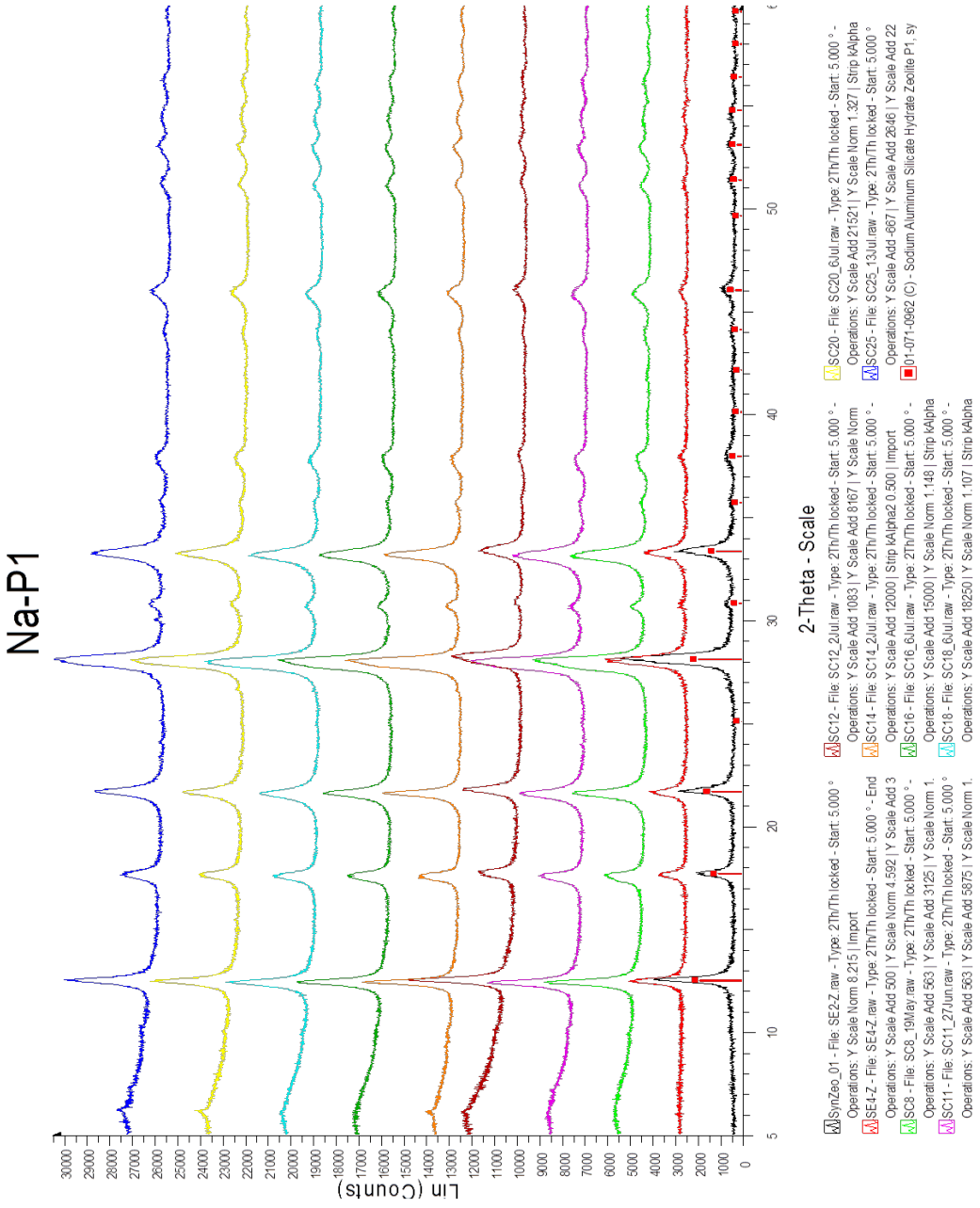
Na-P1
Lin (Counts)
2-Theta - Scale
SynZeo_01 - File: SE2-Z.raw - Type: 2Th/Th locked - Start: 5.000 ° - Operations: Y Scale Norm 8.215 | Import
SE4-Z - File: SE4-Z.raw - Type: 2Th/Th locked - Start: 5.000 ° - End
Operations: Y Scale Add 500 | Y Scale Norm 4.592 | Y Scale Add 3
SC8 - File: SC8_19May.raw - Type: 2Th/Th locked - Start: 5.000 ° - Operations: Y Scale Add 563 | Y Scale Norm 1.
SC11 - File: SC11_27Jun.raw - Type: 2Th/Th locked - Start: 5.000 ° - Operations: Y Scale Add 563 | Y Scale Norm 1.
SC12 - File: SC12_2Jul.raw - Type: 2Th/Th locked - Start: 5.000 ° - Operations: Y Scale Add 1083 | Y Scale Add 8167 | Y Scale Norm
SC14 - File: SC14_2Jul.raw - Type: 2Th/Th locked - Start: 5.000 ° - Operations: Y Scale Add 12000 | Strip kAlpha2 0.500 | Import
SC16 - File: SC16_6Jul.raw - Type: 2Th/Th locked - Start: 5.000 ° - Operations: Y Scale Add 15000 | Y Scale Norm 1.148 | Strip kAlpha
SC18 - File: SC18_6Jul.raw - Type: 2Th/Th locked - Start: 5.000 ° - Operations: Y Scale Add 18250 | Y Scale Norm 1.107 | Strip kAlpha
SC20 - File: SC20_6Jul.raw - Type: 2Th/Th locked - Start: 5.000 ° - Operations: Y Scale Add 21521 | Y Scale Norm 1.327 | Strip kAlpha
SC25 - File: SC25_13Jul.raw - Type: 2Th/Th locked - Start: 5.000 ° Operations: Y Scale Add -667 | Y Scale Add 2646 | Y Scale Add 22
01-071-0962 (C) - Sodium Aluminum Silicate Hydrate Zeolite P1, sy

Figure 9.2

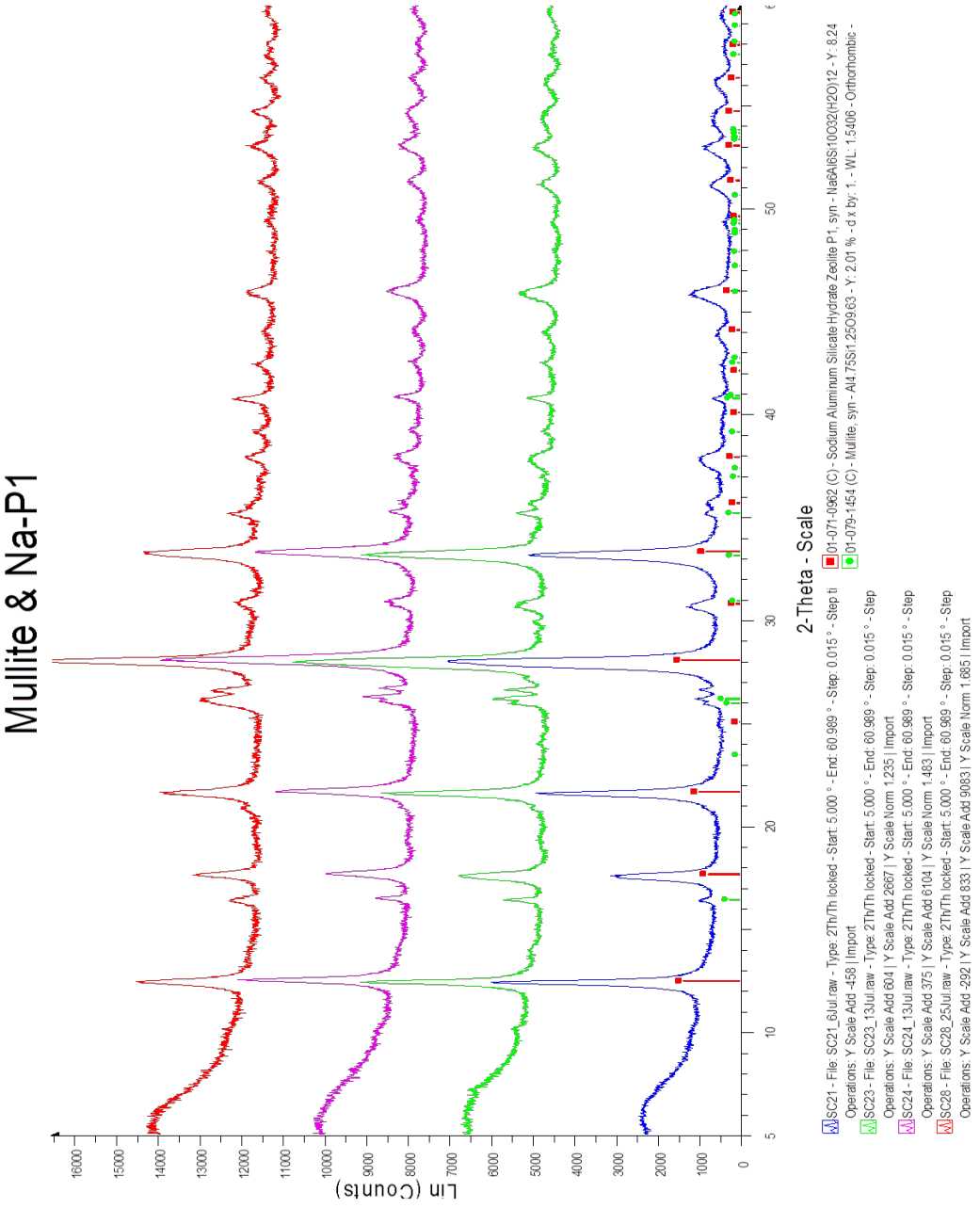
Mullite & Na-P1
Lin (Counts)
2-Theta - Scale
SC21 - File: SC21_6Jul.raw - Type: 2Th/Th locked - Start: 5.000 ° - End: 60.989 ° - Step: 0.015 ° - Step ti
Operations: Y Scale Add -458 | Import
SC23 - File: SC23_13Jul.raw - Type: 2Th/Th locked - Start: 5.000 ° - End: 60.989 ° - Step: 0.015 ° - Step
Operations: Y Scale Add 604 | Y Scale Add 2667 | Y Scale Norm 1.235 | Import
SC24 - File: SC24_13Jul.raw - Type: 2Th/Th locked - Start: 5.000 ° - End: 60.989 ° - Step: 0.015 ° - Step
Operations: Y Scale Add 375 | Y Scale Add 6104 | Y Scale Norm 1.483 | Import
SC28 - File: SC28_25Jul.raw - Type: 2Th/Th locked - Start: 5.000 ° - End: 60.989 ° - Step: 0.015 ° - Step
Operations: Y Scale Add -292 | Y Scale Add 833 | Y Scale Add 9083 | Y Scale Norm 1.085 | Import
01-071-0962 (C) - Sodium Aluminum Silicate Hydrate Zeolite P1, syn - Na6Al6Si10O32(H2O)12 - Y: 8.24
01-079-1454 (C) - Mullite, syn - Al4.75Si1.25O9.63 - Y: 2.01 % - d x by: 1. - WL: 1.5406 - Orthorhombic -

Figure 9.3

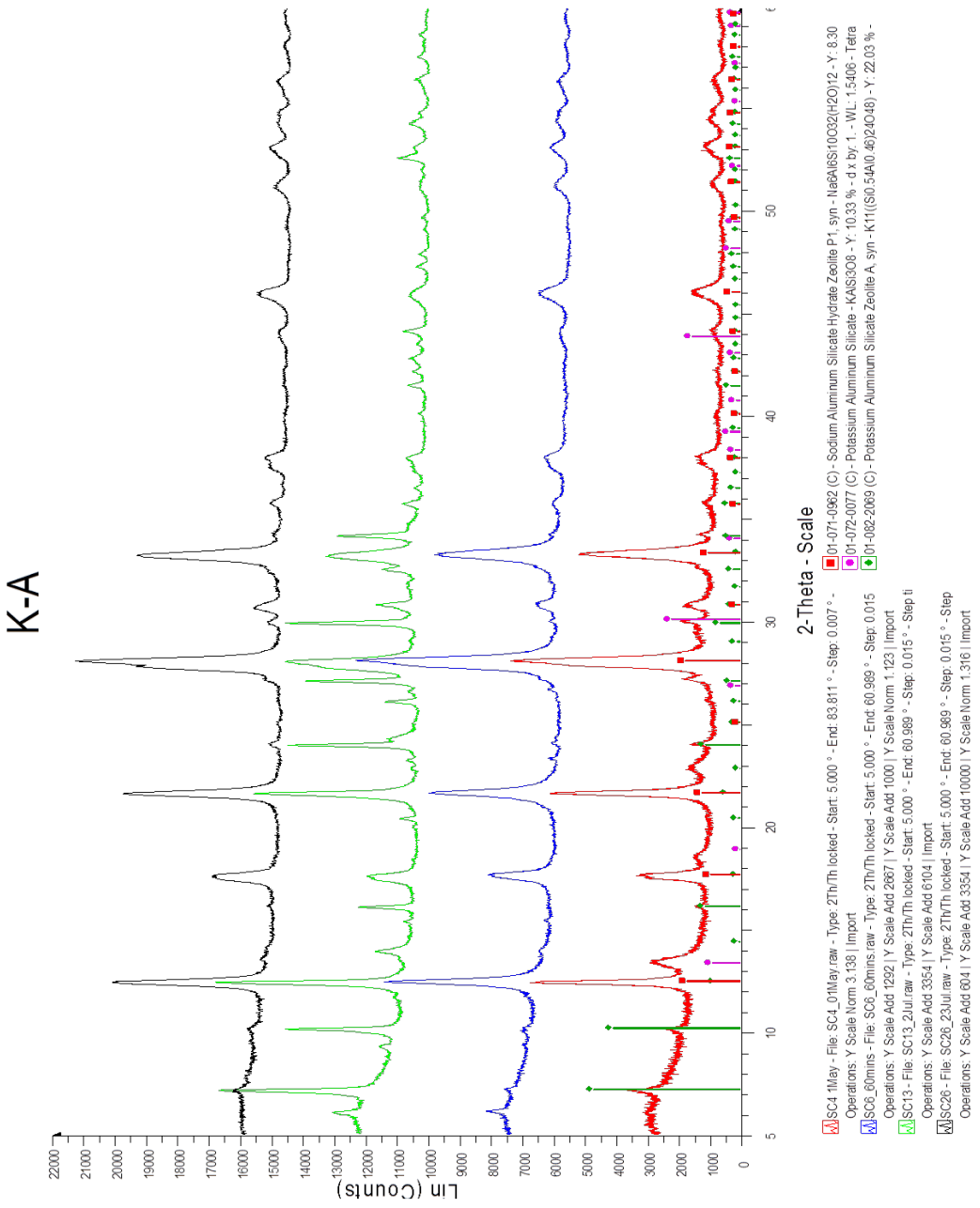
K-A
Lin (Counts)
2-Theta - Scale
SC4 1May - File: SC4_01May.raw - Type: 2Th/Th locked - Start: 5.000 ° - End: 83.811 ° - Step: 0.007 ° -
Operations: Y Scale Norm 3.138 | Import
SC6_60mins - File: SC6_60mins.raw - Type: 2Th/Th locked - Start: 5.000 ° - End: 60.989 ° - Step: 0.015
Operations: Y Scale Add 1292 | Y Scale Add 2667 | Y Scale Add 1000 | Y Scale Norm 1.123 | Import
SC13 - File: SC13_2ul.raw - Type: 2Th/Th locked - Start: 5.000 ° - End: 60.989 ° - Step: 0.015 ° - Step ti
Operations: Y Scale Add 3354 | Y Scale Add 6104 | Import
SC26 - File: SC26_23ul.raw - Type: 2Th/Th locked - Start: 5.000 ° - End: 60.989 ° - Step: 0.015 ° - Step
Operations: Y Scale Add 604 | Y Scale Add 3354 | Y Scale Add 10000 | Y Scale Norm 1.316 | Import
01-071-0962 (C) - Sodium Aluminum Silicate Hydrate Zeolite P1, syn - Na6Al6Si10O32(H2O)12 - Y: 8.30
01-072-0077 (C) - Potassium Aluminum Silicate - KAlSi3O8 - Y: 10.33 % - d x by: 1. - WL: 1.5406 - Tetra
01-082-2069 (C) - Potassium Aluminum Silicate Zeolite A, syn - K11((Si0.5Al0.46)24O48) - Y: 22.03 % -

Figure 9.4

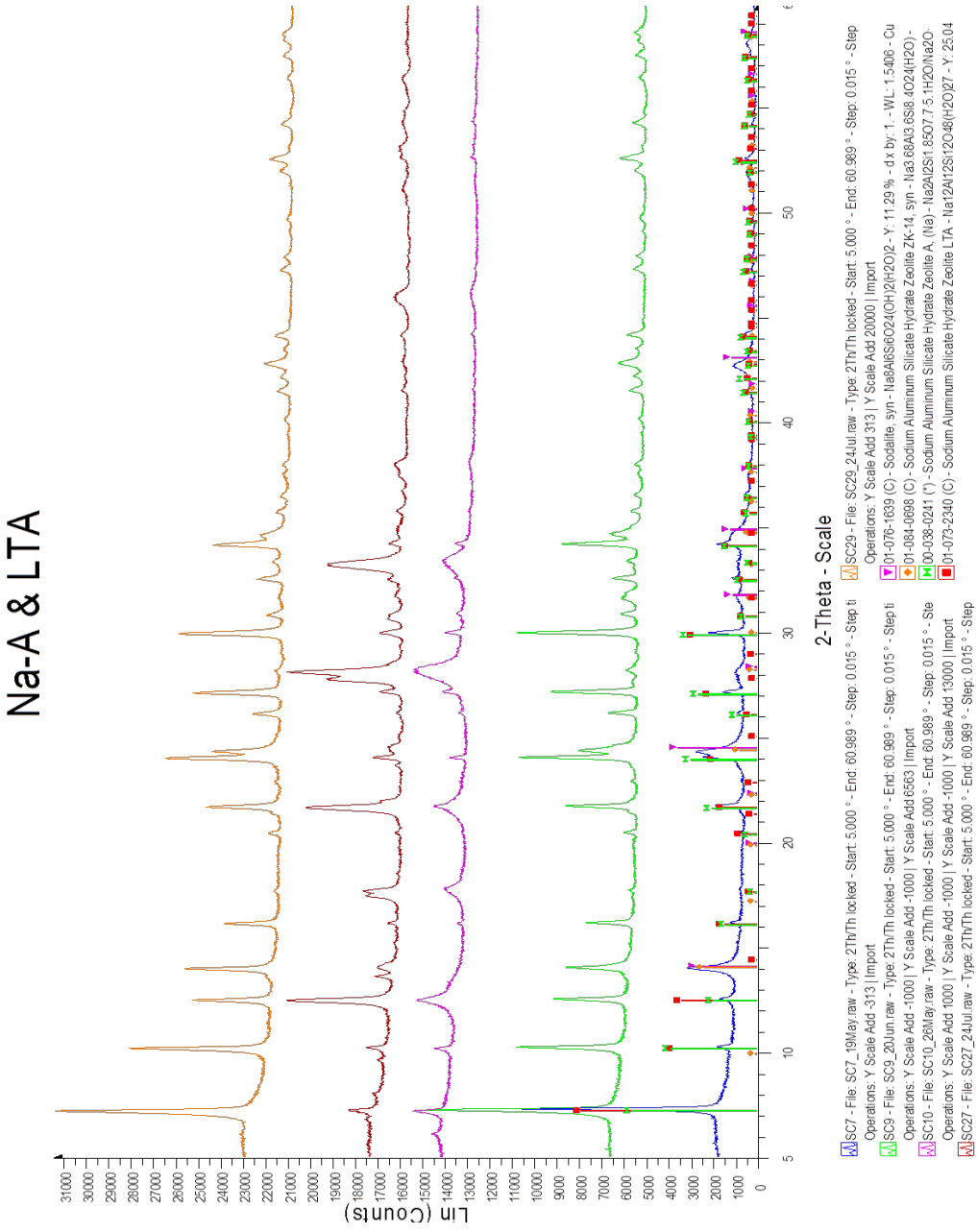
Na-A & LTA
Lin (Counts)
2-Theta - Scale
SC7 - File: SC7_19May.raw - Type: 2Th/Th locked - Start: 5.000 ° - End: 60.989 ° - Step: 0.015 ° - Step ti
Operations: Y Scale Add -313 | Import
SC9 - File: SC9_20Jun.raw - Type: 2Th/Th locked - Start: 5.000 ° - End: 60.989 ° - Step: 0.015 ° - Step ti
Operations: Y Scale Add -1000 | Y Scale Add 6563 | Import
SC10 - File: SC10_26May.raw - Type: 2Th/Th locked - Start: 5.000 ° - End: 60.989 ° - Step: 0.015 ° - Ste
Operations: Y Scale Add 1000 | Y Scale Add -1000 | Y Scale Add 13000 | Import
SC27 - File: SC27_24Jul.raw - Type: 2Th/Th locked - Start: 5.000 ° - End: 60.989 ° - Step: 0.015 ° - Step
Operations: Y Scale Add -125 | Y Scale Add 15188 | Import
SC29 - File: SC29_24Jul.raw - Type: 2Th/Th locked - Start: 5.000 ° - End: 60.989 ° - Step: 0.015 ° - Step
Operations: Y Scale Add 313 | Y Scale Add 20000 | Import
01-076-1639 (C) - Sodalite, syn - Na8Al6Si6O24(OH)2(H2O)2 - Y: 11.29 % - d x by: 1. - WL: 1.5406 - Cu
01-084-0698 (C) - Sodium Aluminum Silicate Hydrate Zeolite Zk-14, syn - Na3.68Al3.6Si8.4O24(H2O) -
00-038-0241 (*) - Sodium Aluminum Silicate Hydrate Zeolite A, (Na) - Na2Al2Si1.85O7.7.5.1H2O/Na2O·
01-073-2340 (C) - Sodium Aluminum Silicate Hydrate Zeolite LTA - Na12Al12Si12O48(H2O)27 - Y: 25.04

Figure 9.5

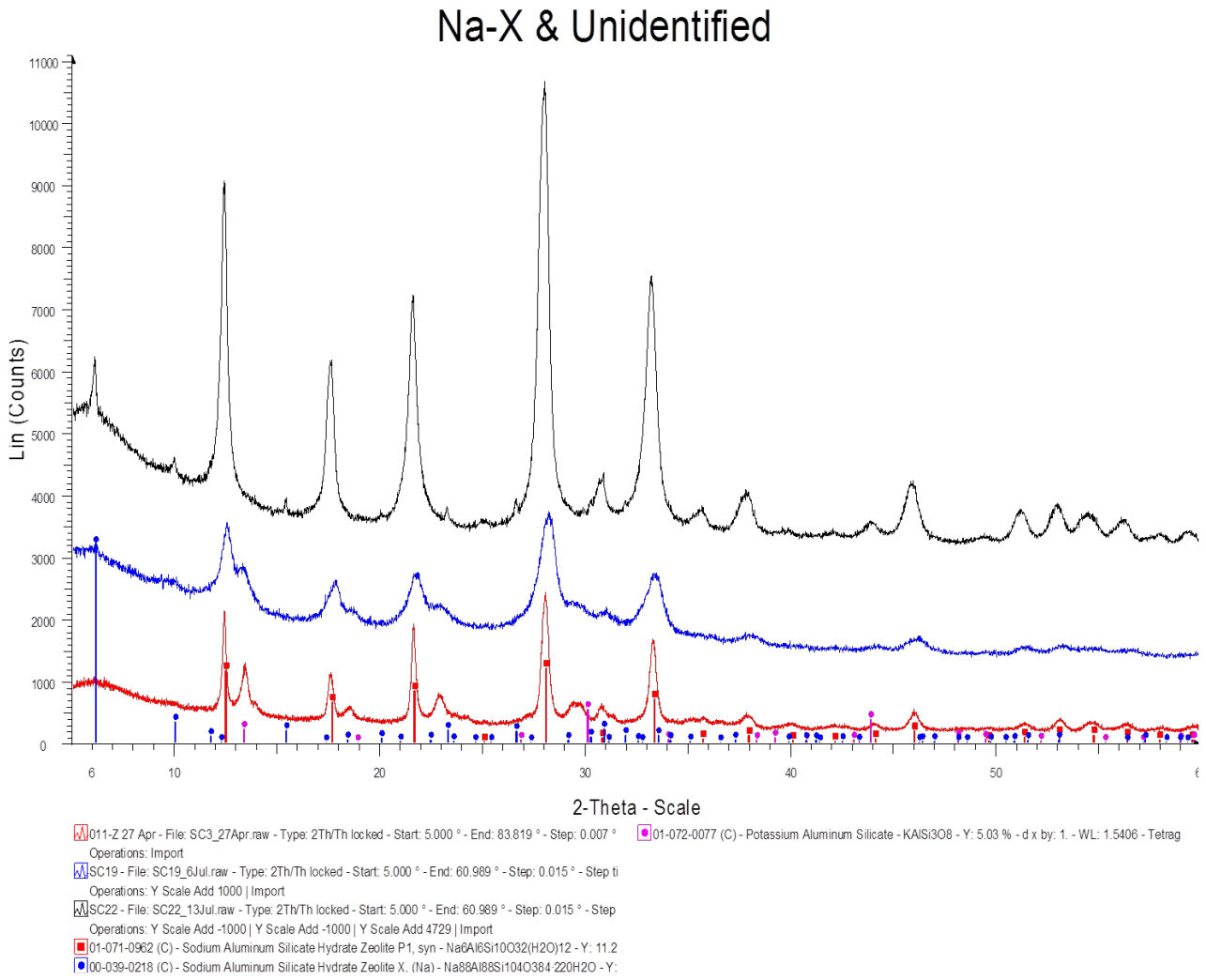
Na-X & Unidentified
Lin (Counts)
11000
10000
9000
8000
7000
6000
5000
4000
3000
2000
1000
0
6
10
20
30
40
50
2-Theta - Scale
011-Z 27 Apr - File: SC3_27Apr.raw - Type: 2Th/Th locked - Start: 5.000 ° - End: 83.819 ° - Step: 0.007 °
Operations: Import
01-072-0077 (C) - Potassium Aluminum Silicate - KAlSi3O8 - Y: 5.03 % - d x by: 1. - WL: 1.5406 - Tetrag
SC19 - File: SC19_6Jul.raw - Type: 2Th/Th locked - Start: 5.000 ° - End: 60.989 ° - Step: 0.015 ° - Step ti
Operations: Y Scale Add 1000 | Import
SC22 - File: SC22_13Jul.raw - Type: 2Th/Th locked - Start: 5.000 ° - End: 60.989 ° - Step: 0.015 ° - Step
Operations: Y Scale Add -1000 | Y Scale Add -1000 | Y Scale Add 4729 | Import
01-071-0962 (C) - Sodium Aluminum Silicate Hydrate Zeolite P1, syn - Na6Al6Si10O32(H2O)12 - Y: 11.2
00-039-0218 (C) - Sodium Aluminum Silicate Hydrate Zeolite X, (Na) - Na88Al88Si104O384·220H2O - Y:

Figure 9.6